

Homogeneous versus Spiral Phases of Hole-doped Antiferromagnets: A Systematic Effective Field Theory Investigation

C. Brügger^a, C. P. Hofmann^b, F. Kämpfer^a, M. Pepe^c,
and U.-J. Wiese^a

^a Institute for Theoretical Physics, Bern University
Sidlerstrasse 5, CH-3012 Bern, Switzerland

^b Facultad de Ciencias, Universidad de Colima
Bernal Díaz del Castillo 340, Colima C.P. 28045, Mexico

^c Istituto Nazionale di Fisica Nucleare and
Dipartimento di Fisica, Università di Milano-Bicocca
3 Piazza della Scienza, 20126 Milano, Italy

September 28, 2006

Abstract

Using the low-energy effective field theory for magnons and holes — the condensed matter analog of baryon chiral perturbation theory for pions and nucleons in QCD — we study different phases of doped antiferromagnets. We systematically investigate configurations of the staggered magnetization that provide a constant background field for doped holes. The most general configuration of this type is either constant itself or it represents a spiral in the staggered magnetization. Depending on the values of the low-energy parameters, a homogeneous phase, a spiral phase, or an inhomogeneous phase is energetically favored. The reduction of the staggered magnetization upon doping is also investigated.

1 Introduction

The precursors of high-temperature superconductors [1] are doped antiferromagnets with a spontaneously broken global $SU(2)_s$ spin symmetry and with magnons as the corresponding Goldstone bosons. The effect of antiferromagnetic spin fluctuations on the dynamics of doped holes has been investigated in great detail in the condensed matter literature [2, 3, 4, 5, 6, 7, 8, 9, 10, 11, 12, 13, 14, 15, 16, 17, 18, 19, 20, 21, 22, 23, 24, 25, 26, 27, 28, 29, 30, 31, 32, 33, 34, 35, 36, 37, 38, 39, 40, 41, 42, 43]. Using a variety of numerical and analytic techniques, a wide range of interesting phenomena has been investigated in doped antiferromagnets. In particular, it was suggested that spiral phases with an inhomogeneous staggered magnetization may replace the Néel phase of the undoped antiferromagnet even at arbitrarily small doping [7, 11, 19, 22, 24, 25, 26, 27, 28, 29, 32, 33, 36, 37, 38, 39, 40, 42, 43]. In a spiral phase the staggered magnetization develops a helix structure, and the Néel ordered antiferromagnet thus turns into a helimagnet. Other inhomogeneities — most important stripes — have also attracted a lot of attention [44]. Unfortunately, away from half-filling, the microscopic Hubbard and t - J models cannot be simulated reliably due to a severe fermion sign problem. Also analytic calculations are usually not fully systematic but suffer from uncontrolled approximations. Consequently, most results for these strongly correlated systems remain, at least to some extent, debatable. While this may seem unavoidable taking into account the complicated nonperturbative dynamics of these systems, a systematic effective field theory approach allows us to reach some unambiguous conclusions at least for lightly doped systems. While some results of this paper have been derived before using less rigorous methods, the effective field theory derivation is still very useful, because it is reliable and particularly transparent.

Particle physicists are facing the challenges of strongly correlated systems in studies of the strong interactions between quarks and gluons. Just like an undoped antiferromagnet, the QCD vacuum has a spontaneously broken global symmetry — in that case the $SU(2)_L \otimes SU(2)_R$ chiral symmetry — which gives rise to three Goldstone pions — the analogs of the magnons in an antiferromagnet. The QCD analog of the doped holes carrying electric charge are the nucleons carrying baryon number. Just as simulating the Hubbard model at non-zero doping is prevented by a fermion sign problem, simulating QCD at non-zero baryon density is prevented by a severe complex action problem. For this reason, lattice QCD is presently limited to simulating individual particles propagating in the QCD vacuum. Although simulations of the QCD vacuum do not suffer from the complex action problem, they are still very demanding, especially in the physical regime of small quark masses. Fortunately, a systematic effective field theory [45, 46, 47, 48] — chiral perturbation theory — is extremely successful in describing the low-energy physics in this regime. In chiral perturbation theory not quarks and gluons but pions and nucleons are the fundamental degrees of freedom. Although the effective theory is not renormalizable, it allows a systematic low-energy expansion with only a finite number of a priori un-

known low-energy parameters entering at each order. The values of the low-energy parameters can be determined from experiments or from lattice QCD simulations. Chiral perturbation theory provides us with precise predictions for the low-energy pion physics, which would be practically impossible to derive directly from QCD. Baryon chiral perturbation theory [49, 50, 51, 52, 53] extends these successes to the low-energy physics of both pions and nucleons. At present, a fully systematic power-counting scheme seems to exist only for the sector with a single nucleon [53]. Still, few-nucleon systems have also been treated quantitatively [54, 55, 56, 57, 58]. The QCD analog of a spiral phase in a doped antiferromagnet is a pion condensate in nuclear matter [59, 60, 61, 62, 63, 64].

The systematic technique of chiral perturbation theory is not limited to QCD but can be applied to any system with Goldstone bosons. Indeed, systematic low-energy effective theories have been very successful in describing the dynamics of magnons in both ferro- and antiferromagnets [9, 10, 13, 23, 30, 35, 65, 66, 67, 68, 69]. In [70, 71] we have extended the pure magnon effective field theory by including charge carriers. The resulting effective theory for magnons and doped holes is the condensed matter analog of baryon chiral perturbation theory. The effective theory incorporates important experimental as well as theoretical results, such as the location of hole pockets at lattice momenta $(\frac{\pi}{2a}, \pm\frac{\pi}{2a})$ which follows from angle resolved photoemission spectroscopy (ARPES) experiments [72, 73, 74, 75] as well as from theoretical investigations of Hubbard or t - J -like models [6, 7, 20, 41]. Recently, we have used the effective theory to derive the magnon-mediated forces between two isolated holes in an otherwise undoped system [71, 76]. Remarkably, the Schrödinger equation corresponding to the one-magnon exchange potential can be solved analytically and gives rise to an infinite number of bound states. It remains to be seen if these isolated hole pairs are related to the preformed Cooper pairs of high-temperature superconductivity. In this paper, we use the effective theory to investigate the regime of small doping. This is possible analytically if the 4-fermion contact interactions between doped holes are weak and can be treated perturbatively. Whether this is indeed the case depends on the concrete magnetic material under consideration. It should be noted that the 4-fermion couplings between doped holes in the effective theory may well be small, although the microscopic on-site Coulomb repulsion U in the Hubbard model or the exchange coupling J in the t - J model which cause antiferromagnetism are strong. In particular, in the effective theory antiferromagnetism arises independent of the strength of the remnant 4-fermion couplings between doped holes. Assuming that the 4-fermion couplings can be treated perturbatively, the effective theory predicts both homogeneous and spiral phases, depending on the specific values of the low-energy parameters.

The paper is organized as follows. In section 2 the effective theory of magnons and holes as well as the nonlinear realization of the spontaneously broken $SU(2)_s$ spin symmetry are reviewed. The holes interact with the Goldstone bosons via a $U(1)_s$ “gauge” field and two “charged” vector fields composed of magnons. The

gauge group $U(1)_s$ and the corresponding “charge” refer to the unbroken subgroup of $SU(2)_s$. In section 3 we consider the most general magnon field that gives rise to constant gauge and charged vector fields and thus to a homogeneous background for the doped holes. These magnon fields turn out either to be homogeneous themselves or to form a spiral in the staggered magnetization. A particular magnon field which gives rise to inhomogeneous composite gauge and charged vector fields — a so-called double spiral — is also discussed. In section 4 homogeneous and spiral phases are investigated. The effect of weak 4-fermion contact interactions is investigated in section 5 using perturbation theory and — depending on the values of the low-energy parameters — it is determined which phase is energetically favored. In section 6 the reduction of the staggered magnetization upon doping is calculated both for the homogeneous and spiral phases. Section 7 contains an outlook as well as our conclusions. In an appendix we prove that the most general configuration of the staggered magnetization that provides a constant background field for the doped holes is either constant itself or represents a spiral.

2 Systematic Low-Energy Effective Field Theory for Magnons and Holes

In order to make this paper self-contained, in this section we review the effective theory for magnons and holes constructed in [70, 71] which is based on the pure magnon effective theory of [10, 13, 23, 30, 35, 65, 66, 67, 68].

The staggered magnetization of an antiferromagnet is described by a unit-vector field

$$\vec{e}(x) = (\sin \theta(x) \cos \varphi(x), \sin \theta(x) \sin \varphi(x), \cos \theta(x)), \quad (2.1)$$

in the coset space $SU(2)_s/U(1)_s = S^2$, with $x = (x_1, x_2, t)$ denoting a point in (2+1)-dimensional space-time. For our purposes it is more convenient (but completely equivalent) to use a $\mathbb{C}P(1)$ representation in terms of 2×2 Hermitean projection matrices $P(x)$ that obey

$$P(x) = \frac{1}{2}(\mathbb{1} + \vec{e}(x) \cdot \vec{\sigma}), \quad P(x)^\dagger = P(x), \quad \text{Tr}P(x) = 1, \quad P(x)^2 = P(x), \quad (2.2)$$

where $\vec{\sigma}$ are the Pauli matrices. The relevant symmetries are realized as follows

$$\begin{aligned} SU(2)_s : & \quad P(x)' = gP(x)g^\dagger, \\ D_i : & \quad D_i P(x) = \mathbb{1} - P(x), \\ O : & \quad O P(x) = P(Ox), \quad Ox = (-x_2, x_1, t), \\ R : & \quad R P(x) = P(Rx), \quad Rx = (x_1, -x_2, t), \\ T : & \quad T P(x) = \mathbb{1} - P(Tx), \quad Tx = (x_1, x_2, -t). \end{aligned} \quad (2.3)$$

Here $g \in SU(2)_s$ is a matrix that implements the global spin symmetry which is spontaneously broken down to $U(1)_s$, D_i denotes the displacement by one lattice spacing in the i -direction, and O , R , and T denote 90 degrees spatial rotations, spatial reflections, and time-reversal, respectively.

In order to couple doped holes to the magnons, a nonlinear realization of the $SU(2)_s$ symmetry was constructed in [70]. The magnon field is diagonalized by a unitary transformation $u(x) \in SU(2)_s$, i.e.

$$u(x)P(x)u(x)^\dagger = \frac{1}{2}(\mathbb{1} + \sigma_3) = \begin{pmatrix} 1 & 0 \\ 0 & 0 \end{pmatrix}, \quad u_{11}(x) \geq 0, \quad (2.4)$$

with

$$u(x) = \begin{pmatrix} \cos(\frac{1}{2}\theta(x)) & \sin(\frac{1}{2}\theta(x)) \exp(-i\varphi(x)) \\ -\sin(\frac{1}{2}\theta(x)) \exp(i\varphi(x)) & \cos(\frac{1}{2}\theta(x)) \end{pmatrix}. \quad (2.5)$$

The transformation $u(x)$ describes a rotation of the local staggered magnetization vector $\vec{e}(x)$ into the 3-direction. Since $u(x)$ is more directly related to $P(x)$ than to $\vec{e}(x)$ itself, we have chosen the $\mathbb{C}P(1)$ representation. Under a global $SU(2)_s$ transformation g the diagonalizing field $u(x)$ transforms as

$$u(x)' = h(x)u(x)g^\dagger, \quad u_{11}(x)' \geq 0, \quad (2.6)$$

which defines the nonlinear $U(1)_s$ symmetry transformation

$$h(x) = \exp(i\alpha(x)\sigma_3), \quad (2.7)$$

that acts like a gauge transformation in the unbroken subgroup $U(1)_s$. The local symmetry transformation $h(x)$ depends on the global transformation g as well as on the local staggered magnetization $P(x)$ from which it inherits its x -dependence. Under the displacement symmetry D_i one obtains

$$D_i u(x) = \tau(x)u(x), \quad \tau(x) = \begin{pmatrix} 0 & -\exp(-i\varphi(x)) \\ \exp(i\varphi(x)) & 0 \end{pmatrix}. \quad (2.8)$$

The way in which the global $SU(2)_s$ spin symmetry disguises itself as a local symmetry in the unbroken $U(1)_s$ subgroup is characteristic for any systematic effective field theory of Goldstone bosons. The nonlinear realization of spontaneously broken continuous global symmetries has been discussed in full generality in the pioneering work of Callan, Coleman, Wess, and Zumino [45, 46]. Following their general scheme, doped holes are derivatively coupled to the magnons. In fact, the holes are ‘‘charged’’ under the local $U(1)_s$ symmetry and transform with the nonlinear transformation $h(x)$. In order to couple holes to the magnons it is necessary to introduce the anti-Hermitian traceless field

$$v_\mu(x) = u(x)\partial_\mu u(x)^\dagger, \quad (2.9)$$

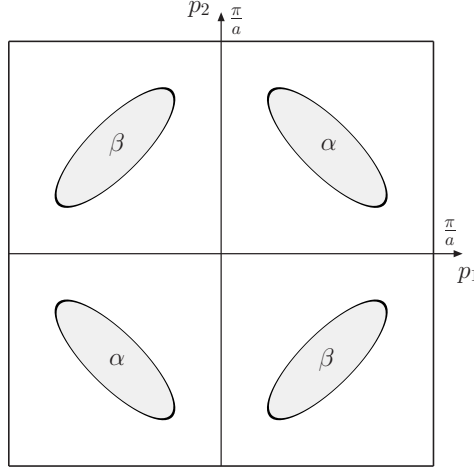


Figure 1: *Elliptically shaped hole pockets centered at $(\pm\frac{\pi}{2a}, \pm\frac{\pi}{2a})$. Two pockets centered at k^f and $k^f + (\frac{\pi}{a}, \frac{\pi}{a})$ combine to form the pockets for the flavors $f = \alpha, \beta$.*

which obeys the following transformation rules

$$\begin{aligned}
SU(2)_s : \quad & v_\mu(x)' = h(x)[v_\mu(x) + \partial_\mu]h(x)^\dagger, \\
D_i : \quad & {}^{D_i}v_\mu(x) = \tau(x)[v_\mu(x) + \partial_\mu]\tau(x)^\dagger, \\
O : \quad & {}^Ov_i(x) = \varepsilon_{ij}v_j(Ox), \quad {}^Ov_t(x) = v_t(Ox), \\
R : \quad & {}^Rv_1(x) = v_1(Rx), \quad {}^Rv_2(x) = -v_2(Rx), \quad {}^Rv_t(x) = v_t(Rx), \\
T : \quad & {}^Tv_j(x) = {}^{D_i}v_j(Tx), \quad {}^Tv_t(x) = -{}^{D_i}v_t(Tx).
\end{aligned} \tag{2.10}$$

Writing

$$v_\mu(x) = iv_\mu^a(x)\sigma_a, \quad v_\mu^\pm(x) = v_\mu^1(x) \mp iv_\mu^2(x), \tag{2.11}$$

the field $v_\mu(x)$ decomposes into an Abelian “gauge” field $v_\mu^3(x)$ and two “charged” vector fields $v_\mu^\pm(x)$, which transform as

$$v_\mu^3(x)' = v_\mu^3(x) - \partial_\mu\alpha(x), \quad v_\mu^\pm(x)' = v_\mu^\pm(x) \exp(\pm 2i\alpha(x)), \tag{2.12}$$

under $SU(2)_s$.

ARPES measurements [72, 73, 74, 75] as well as theoretical calculations in t - J -like models [6, 20, 41] have revealed that at small doping holes occur in pockets centered at $k^\alpha = (\frac{\pi}{2a}, \frac{\pi}{2a})$ and $k^\beta = (\frac{\pi}{2a}, -\frac{\pi}{2a})$ in the Brillouin zone. The elliptically shaped hole pockets are illustrated in figure 1. The effective field theory is defined in the space-time continuum and the holes are described by Grassmann-valued fields $\psi_s^f(x)$ carrying a “flavor” index $f = \alpha, \beta$ that characterizes the corresponding hole pocket. The index $s = \pm$ denotes spin parallel (+) or antiparallel (−) to the local staggered magnetization. Following [70, 71], under the various symmetry operations

the hole fields transform as

$$\begin{aligned}
SU(2)_s : \quad & \psi_{\pm}^f(x)' = \exp(\pm i\alpha(x))\psi_{\pm}^f(x), \\
U(1)_Q : \quad & \mathcal{Q}\psi_{\pm}^f(x) = \exp(i\omega)\psi_{\pm}^f(x), \\
D_i : \quad & D_i\psi_{\pm}^f(x) = \mp \exp(ik_i^f a) \exp(\mp i\varphi(x))\psi_{\mp}^f(x), \\
O : \quad & O\psi_{\pm}^{\alpha}(x) = \mp \psi_{\pm}^{\beta}(Ox), \quad O\psi_{\pm}^{\beta}(x) = \psi_{\pm}^{\alpha}(Ox), \\
R : \quad & R\psi_{\pm}^{\alpha}(x) = \psi_{\pm}^{\beta}(Rx), \quad R\psi_{\pm}^{\beta}(x) = \psi_{\pm}^{\alpha}(Rx), \\
T : \quad & T\psi_{\pm}^f(x) = \mp \exp(\mp i\varphi(Tx))\psi_{\pm}^{f\dagger}(Tx), \\
& T\psi_{\pm}^{f\dagger}(x) = \pm \exp(\pm i\varphi(Tx))\psi_{\pm}^f(Tx).
\end{aligned} \tag{2.13}$$

Here $U(1)_Q$ is the fermion number symmetry of the holes. Interestingly, in the effective continuum theory the location of holes in lattice momentum space manifests itself as a ‘‘charge’’ k_i^f under the displacement symmetry D_i .

Once the relevant low-energy degrees of freedom have been identified, and the transformation rules of the corresponding fields have been understood, the construction of the effective action is uniquely determined. The low-energy effective action of magnons and holes is constructed as a derivative expansion. At low energies terms with a small number of derivatives dominate the dynamics. Since the holes are heavy nonrelativistic fermions, one time-derivative counts like two spatial derivatives. Here we limit ourselves to terms with at most one temporal or two spatial derivatives. One then constructs all terms consistent with the symmetries listed above. The effective action can be written as

$$S[\psi_{\pm}^{f\dagger}, \psi_{\pm}^f, P] = \int d^2x dt \sum_{n_{\psi}} \mathcal{L}_{n_{\psi}}, \tag{2.14}$$

where n_{ψ} denotes the number of fermion fields that the various terms contain. The leading terms in the pure magnon sector take the form

$$\begin{aligned}
\mathcal{L}_0 &= \rho_s \text{Tr} \left[\partial_i P \partial_i P + \frac{1}{c^2} \partial_t P \partial_t P \right] \\
&= \frac{\rho_s}{2} \left(\partial_i \vec{e} \cdot \partial_i \vec{e} + \frac{1}{c^2} \partial_t \vec{e} \cdot \partial_t \vec{e} \right) = 2\rho_s \left(v_i^+ v_i^- + \frac{1}{c^2} v_t^+ v_t^- \right).
\end{aligned} \tag{2.15}$$

Here ρ_s is the spin stiffness and c is the spinwave velocity. The leading terms with two fermion fields (containing at most one temporal or two spatial derivatives) are given by

$$\begin{aligned}
\mathcal{L}_2 = \sum_{\substack{f=\alpha,\beta \\ s=+,-}} & \left[M\psi_s^{f\dagger}\psi_s^f + \psi_s^{f\dagger} D_t \psi_s^f \right. \\
& + \frac{1}{2M'} D_i \psi_s^{f\dagger} D_i \psi_s^f + \sigma_f \frac{1}{2M''} (D_1 \psi_s^{f\dagger} D_2 \psi_s^f + D_2 \psi_s^{f\dagger} D_1 \psi_s^f) \\
& + \Lambda (\psi_s^{f\dagger} v_1^s \psi_{-s}^f + \sigma_f \psi_s^{f\dagger} v_2^s \psi_{-s}^f) \\
& \left. + N_1 \psi_s^{f\dagger} v_i^s v_i^{-s} \psi_s^f + \sigma_f N_2 (\psi_s^{f\dagger} v_1^s v_2^{-s} \psi_s^f + \psi_s^{f\dagger} v_2^s v_1^{-s} \psi_s^f) \right].
\end{aligned} \tag{2.16}$$

It should be noted that $v_i^\pm(x)$ contains a spatial derivative, such that magnons and holes are indeed derivatively coupled. In eq.(2.16) M is the rest mass and M' and M'' are the kinetic masses of a hole, Λ is a hole-one-magnon, and N_1 and N_2 are hole-two-magnon couplings, which all take real values. The sign σ_f is $+$ for $f = \alpha$ and $-$ for $f = \beta$. The covariant derivative takes the form

$$D_\mu \psi_\pm^f(x) = \partial_\mu \psi_\pm^f(x) \pm i v_\mu^3(x) \psi_\pm^f(x). \quad (2.17)$$

The leading terms with four fermion fields are given by

$$\begin{aligned} \mathcal{L}_4 = \sum_{s=+,-} \left\{ \frac{G_1}{2} (\psi_s^{\alpha\dagger} \psi_s^\alpha \psi_{-s}^{\alpha\dagger} \psi_{-s}^\alpha + \psi_s^{\beta\dagger} \psi_s^\beta \psi_{-s}^{\beta\dagger} \psi_{-s}^\beta) \right. \\ + G_2 \psi_s^{\alpha\dagger} \psi_s^\alpha \psi_s^{\beta\dagger} \psi_s^\beta + G_3 \psi_s^{\alpha\dagger} \psi_s^\alpha \psi_{-s}^{\beta\dagger} \psi_{-s}^\beta \\ + G_4 \left[\psi_s^{\alpha\dagger} \psi_s^\alpha \sum_{s'=+,-} (\psi_{s'}^{\beta\dagger} v_1^{s'} \psi_{-s'}^\beta - \psi_{s'}^{\beta\dagger} v_2^{s'} \psi_{-s'}^\beta) \right. \\ \left. + \psi_s^{\beta\dagger} \psi_s^\beta \sum_{s'=+,-} (\psi_{s'}^{\alpha\dagger} v_1^{s'} \psi_{-s'}^\alpha + \psi_{s'}^{\alpha\dagger} v_2^{s'} \psi_{-s'}^\alpha) \right] \left. \right\}, \quad (2.18) \end{aligned}$$

with the real-valued 4-fermion coupling constants G_1 , G_2 , G_3 , and G_4 . Here we have limited ourselves to terms containing at most one spatial derivative. In principle there are even more contact interactions among the fermions such as 6- and 8-fermion couplings as well as 4-fermion couplings including more derivatives. Some of these terms have been constructed in [71] but play no role in the present work and have hence been suppressed.

Remarkably, the above Lagrangian has an accidental global $U(1)_F$ flavor symmetry that acts as

$$U(1)_F : {}^F \psi_\pm^f(x) = \exp(\sigma_f i \eta) \psi_\pm^f(x). \quad (2.19)$$

This symmetry is not present in the underlying microscopic systems and is indeed explicitly broken by higher-order terms in the effective action. For $c \rightarrow \infty$ the leading terms of the effective action also have an accidental Galilean boost symmetry

$$\begin{aligned} G : \quad {}^G P(x) &= P(Gx), \quad Gx = (\vec{x} - \vec{v} t, t), \\ {}^G \psi_\pm^f(x) &= \exp(i \vec{p}^f \cdot \vec{x} - \omega^f t) \psi_\pm^f(Gx), \\ {}^G \psi_\pm^{f\dagger}(x) &= \psi_\pm^{f\dagger}(Gx) \exp(-i \vec{p}^f \cdot \vec{x} + \omega^f t), \end{aligned} \quad (2.20)$$

with $\vec{p}^f = (p_1^f, p_2^f)$ and ω^f given by

$$\begin{aligned} p_1^f &= \frac{M'}{1 - (M'/M'')^2} \left(v_1 - \sigma_f \frac{M'}{M''} v_2 \right), \quad p_2^f = \frac{M'}{1 - (M'/M'')^2} \left(v_2 - \sigma_f \frac{M'}{M''} v_1 \right), \\ \omega^f &= \frac{p_i^{f2}}{2M'} + \sigma_f \frac{p_1^f p_2^f}{M''} = \frac{M'}{1 - (M'/M'')^2} \left[\frac{1}{2} (v_1^2 + v_2^2) - \sigma_f \frac{M'}{M''} v_1 v_2 \right]. \end{aligned} \quad (2.21)$$

Also the Galilean boost symmetry is explicitly broken at higher orders of the derivative expansion. In the real materials Galilean (or actually Poincaré) invariance is spontaneously broken by the formation of a crystal lattice, with phonons as the corresponding Goldstone bosons. Here we assume that phonons play no major role in the cuprates, and we focus entirely on the magnons. Still, phonons and a spontaneously broken Galilean symmetry could be included in the effective field theory if necessary.

3 Spirals in the Staggered Magnetization

In the following we will consider configurations $\vec{e}(x)$ of the staggered magnetization which — although not necessarily constant themselves — provide a constant background field for the doped holes. We restrict ourselves to time-independent configurations, such that $v_i(x) = 0$. The most general configuration, with $v_i(x)$ constant up to a gauge transformation, represents a spiral in the staggered magnetization. We also discuss a so-called double spiral which gives rise to a non-uniform composite vector field and thus to an inhomogeneous fermion density.

3.1 Spirals with Uniform Composite Vector Fields

Since the holes couple to the composite vector field $v_i(x)$ in a gauge covariant way, it is sufficient to assume that $v_i(x)$ is constant only up to a gauge transformation, i.e.

$$\begin{aligned} v_i^3(x)' &= v_i^3(x) - \partial_i \alpha(x) = \sin^2 \frac{\theta(x)}{2} \partial_i \varphi(x) - \partial_i \alpha(x) = c_i^3, \\ v_i^\pm(x)' &= v_i^\pm(x) \exp(\pm 2i\alpha(x)) \\ &= \frac{1}{2} [\sin \theta(x) \partial_i \varphi(x) \pm i \partial_i \theta(x)] \exp(\mp i(\varphi(x) - 2\alpha(x))) = c_i^\pm, \end{aligned} \quad (3.1)$$

with c_i^3 and c_i^\pm being constant. As shown in the appendix, the most general configuration that leads to a constant $v_i(x)'$ represents a spiral in the staggered magnetization. Furthermore, by an appropriate gauge transformation one can always achieve

$$c_i^+ = c_i^- = c_i \in \mathbb{R}. \quad (3.2)$$

The magnon contribution to the energy density of these configurations is given by

$$\epsilon_m = \frac{\rho_s}{2} \partial_i \vec{e}(x) \cdot \partial_i \vec{e}(x) = 2\rho_s v_i^+(x) v_i^-(x) = 2\rho_s (c_1^2 + c_2^2). \quad (3.3)$$

To be specific, let us consider a concrete family of spiral configurations with

$$\theta(x) = \theta_0, \quad \varphi(x) = k_i x_i, \quad (3.4)$$

which implies

$$v_t(x) = 0, \quad v_i^3(x) = k_i \sin^2 \frac{\theta_0}{2}, \quad v_i^\pm(x) = \frac{k_i}{2} \sin \theta_0 \exp(\mp i k_i x_i). \quad (3.5)$$

Choosing the gauge transformation

$$\alpha(x) = \frac{1}{2} k_i x_i, \quad (3.6)$$

one obtains the constant field

$$\begin{aligned} v_t(x)' &= 0, \quad v_i^3(x)' = v_i^3(x) - \partial_i \alpha(x) = k_i \left(\sin^2 \frac{\theta_0}{2} - \frac{1}{2} \right) = c_i^3, \\ v_i^\pm(x)' &= v_i^\pm(x) \exp(\pm 2i \alpha(x)) = \frac{k_i}{2} \sin \theta_0 = c_i. \end{aligned} \quad (3.7)$$

Hence, comparing with the appendix, in this case we can identify

$$c_i^3 = -\frac{k_i}{2} \cos \theta_0, \quad a = \frac{c_i}{c_i^3} = -\tan \theta_0, \quad (3.8)$$

and the magnon contribution to the energy density is

$$\epsilon_m = 2\rho_s(c_1^2 + c_2^2) = \frac{\rho_s}{2}(k_1^2 + k_2^2) \sin^2 \theta_0. \quad (3.9)$$

3.2 A Double Spiral

For most of this paper we restrict ourselves to configurations of the staggered magnetization which give rise to a homogeneous composite vector field $v_i(x)'$. However, in this subsection we examine a configuration with an inhomogeneous $v_i(x)'$ — the so-called double spiral [19]. Although we will not explore this configuration any further in this work, it is interesting for future investigations. In particular, one can study it in order to figure out whether spirals with constant $v_i(x)'$ may be unstable against developing inhomogeneities.

A particularly simple form of a double spiral is given by

$$\vec{e}(x) = (\sin(k_1 x_1) \cos(k_2 x_2), \sin(k_2 x_2), \cos(k_1 x_1) \cos(k_2 x_2)). \quad (3.10)$$

The magnon contribution to the energy density of the double spiral takes the form

$$\epsilon_m = \frac{\rho_s}{2} \partial_i \vec{e}(x) \cdot \partial_i \vec{e}(x) = \frac{\rho_s}{2} (k_1^2 \cos^2(k_2 x_2) + k_2^2). \quad (3.11)$$

It is straightforward to compute the composite vector field for the double spiral and one obtains

$$\begin{aligned}
v_1^3(x) &= -\frac{k_1 \cos(k_1 x_1) \sin(k_2 x_2) \cos(k_2 x_2)}{2(1 + \cos(k_1 x_1) \cos(k_2 x_2))}, \\
v_1^\pm(x) &= \frac{k_1 \cos(k_2 x_2) [\sin(k_1 x_1) \sin(k_2 x_2) \pm i(\cos(k_1 x_1) + \cos(k_2 x_2))]}{2(1 + \cos(k_1 x_1) \cos(k_2 x_2))}, \\
v_2^3(x) &= \frac{k_2 \sin(k_1 x_1)}{2(1 + \cos(k_1 x_1) \cos(k_2 x_2))}, \\
v_2^\pm(x) &= \frac{k_2 [\cos(k_1 x_1) + \cos(k_2 x_2) \mp i \sin(k_1 x_1) \sin(k_2 x_2)]}{2(1 + \cos(k_1 x_1) \cos(k_2 x_2))}.
\end{aligned} \tag{3.12}$$

As before we perform a gauge transformation

$$v_i^3(x)' = v_i^3(x) - \partial_i \alpha(x), \quad v_i^\pm(x)' = v_i^\pm(x) \exp(\pm 2i\alpha(x)), \tag{3.13}$$

in this case with

$$\exp(2i\alpha(x)) = \frac{\sin(k_1 x_1) \sin(k_2 x_2) - i(\cos(k_1 x_1) + \cos(k_2 x_2))}{1 + \cos(k_1 x_1) \cos(k_2 x_2)}, \tag{3.14}$$

and we obtain the remarkably simple form

$$\begin{aligned}
v_1^3(x)' &= -\frac{k_1}{2} \sin(k_2 x_2), & v_1^\pm(x)' &= \frac{k_1}{2} \cos(k_2 x_2), \\
v_2^3(x)' &= 0, & v_2^\pm(x)' &= \mp i \frac{k_2}{2}.
\end{aligned} \tag{3.15}$$

4 Homogeneous versus Spiral Phases

In this section we calculate the fermionic contribution to the energy density of a configuration with constant $v_i(x)'$ in order to decide which configuration is energetically favored. It will turn out that this depends on the values of the low-energy parameters. For large ρ_s the magnon contribution to the energy density dominates, and a homogeneous phase is favored. In that case, all four hole pockets are equally populated with doped holes of both spin up and spin down. For smaller ρ_s , on the other hand, the fermionic contribution to the energy density dominates and favors a spiral configuration. In this case, only a particular linear combination of spin up and spin down states is occupied by doped holes. If the spiral is oriented along a crystal lattice axis (a zero degree spiral) hole pockets of both types (α and β) are filled with doped holes. On the other hand, if the spiral is oriented along a lattice diagonal (a 45 degrees spiral) either three or one hole pocket are populated. As we will see, the zero degree spiral is realized for intermediate values of ρ_s , while the 45 degrees spiral is unstable against the formation of inhomogeneities in the fermion

density. Interesting calculations of a similar nature were presented in [42, 43] in the context of microscopic t - J -like models. In these works, in a particular parameter range a zero degree spiral has been identified as the most stable configuration. Our effective field theory treatment complements these results in an interesting way. First, it is model-independent and thus applicable to a large variety of microscopic systems, because the most general form of the effective action is taken into account. In addition, it is controlled by a systematic low-energy expansion. Before we discuss homogeneous versus spiral phases, we address the issue of phase separation in the context of the t - J model.

4.1 Stability against Phase Separation

It is well-known that the t - J model shows phase separation for small values of t . In this case the doped holes are heavy. Each hole is surrounded by four bonds which, in the absence of the hole, would carry a negative antiferromagnetic contribution to the energy. In order to minimize the number of broken antiferromagnetic bonds, the holes may accumulate in some region of the lattice, thus leaving an otherwise undoped antiferromagnet behind, i.e. the system undergoes phase separation.

The energy density of the undoped antiferromagnet is ϵ_0 . In the t - J model, which reduces to the Heisenberg model at half-filling, the energy density was determined with a very efficient loop-cluster algorithm as $\epsilon_0 = -0.6693(1)J/a^2$, where J is the exchange coupling and a is the lattice spacing [77]. A doped hole propagating in the antiferromagnet has mass M . Hence, to leading order in the fermion density n , the energy density of a doped antiferromagnet is

$$\epsilon = \epsilon_0 + Mn + \mathcal{O}(n^2). \quad (4.1)$$

When the system phase separates, the doped holes accumulate in some region of volume V' , leaving an otherwise undoped antiferromagnet behind in the remaining volume $V - V'$. If there are no electrons at all in the hole-rich region, each hole occupies an area a^2 and hence $V' = Na^2$, where N is the number of holes. In the t - J model, the unoccupied region of volume V' does not contribute to the energy density, while in the remaining volume $V - V'$ one has the energy density ϵ_0 of an undoped antiferromagnet. Hence, the energy density of a phase separated system is

$$\epsilon_{\text{ps}} = \frac{\epsilon_0(V - V')}{V} = \epsilon_0(1 - a^2n). \quad (4.2)$$

The doped t - J model is thus stable against phase separation as long as

$$\epsilon < \epsilon_{\text{ps}} \Rightarrow M < -\epsilon_0 a^2 = 0.6693(1)J. \quad (4.3)$$

In the t - J model at small t the holes are essentially static, breaking four antiferromagnetic bonds, while ϵ_0 represents the energy of two intact antiferromagnetic

bonds. Hence, for small t one has $M \approx -2\epsilon_0 a^2$ which implies phase separation. However, the hole mass M decreases with increasing t and can even become negative [41]. Hence, for sufficiently large t , one indeed obtains a doped antiferromagnet which is stable against phase separation. It should be noted that a negative rest mass M is not at all problematical from a theoretical point of view. It only means that the doped antiferromagnet has a lower energy than the undoped system. Still, since particle number is conserved, the system cannot lower its energy by creating fermions.

4.2 Fermionic Contribution to the Energy

In this subsection we compute the fermionic contribution to the energy, keeping the parameters c_i^3 and c_i^\pm of the spiral fixed. For the moment, we ignore the 4-fermion couplings. The considerations of this paper are valid only if the 4-fermion couplings are weak and can be treated in perturbation theory. Furthermore, we may neglect the hole-two-magnon vertices proportional to N_1 and N_2 which involve two spatial derivatives and are thus of higher order than the hole-one-magnon vertex proportional to Λ . The Euclidean action of eq.(2.16) then gives rise to the fermion Hamiltonian

$$H = \int d^2x \sum_{\substack{f=\alpha,\beta \\ s=+,-}} \left[M \Psi_s^{f\dagger} \Psi_s^f + \frac{1}{2M'} D_i \Psi_s^{f\dagger} D_i \Psi_s^f + \sigma_f \frac{1}{2M''} (D_1 \Psi_s^{f\dagger} D_2 \Psi_s^f + D_2 \Psi_s^{f\dagger} D_1 \Psi_s^f) + \Lambda (\Psi_s^{f\dagger} v_1^s \Psi_{-s}^f + \sigma_f \Psi_s^{f\dagger} v_2^s \Psi_{-s}^f) \right], \quad (4.4)$$

with the covariant derivative

$$D_i \Psi_\pm^f(x) = \partial_i \Psi_\pm^f(x) \pm i v_i^3(x) \Psi_\pm^f(x). \quad (4.5)$$

Here $\Psi_s^{f\dagger}(x)$ and $\Psi_s^f(x)$ are creation and annihilation operators (not Grassmann numbers) for fermions of flavor $f = \alpha, \beta$ and spin $s = +, -$ (parallel or antiparallel to the local staggered magnetization), which obey canonical anticommutation relations. As before, $\sigma_\alpha = 1$ and $\sigma_\beta = -1$. The above Hamiltonian is invariant against time-independent $U(1)_s$ gauge transformations

$$\begin{aligned} \Psi_\pm^f(x)' &= \exp(\pm i\alpha(x)) \Psi_\pm^f(x), \\ v_i^3(x)' &= v_i^3(x) - \partial_i \alpha(x), \quad v_i^\pm(x)' = v_i^\pm(x) \exp(\pm 2i\alpha(x)). \end{aligned} \quad (4.6)$$

Here we consider holes propagating in the background of a configuration with a spiral in the staggered magnetization. Based on the considerations in the appendix, we can then limit ourselves to

$$v_i^3(x)' = c_i^3, \quad v_i^\pm(x)' = c_i \in \mathbb{R}. \quad (4.7)$$

Hence, after the gauge transformation, the fermions experience a constant composite vector field $v_i(x)'$. The Hamiltonian can then be diagonalized by going to momentum space. Since magnon exchange does not mix the flavors, the Hamiltonian can be considered separately for $f = \alpha$ and $f = \beta$, but it still mixes spin $s = +$ with $s = -$. The single-particle Hamiltonian for holes with spatial momentum $\vec{p} = (p_1, p_2)$ takes the form

$$H^f(\vec{p}) = \begin{pmatrix} M + \frac{(p_i - c_i^3)^2}{2M'} + \sigma_f \frac{(p_1 - c_1^3)(p_2 - c_2^3)}{M''} & \Lambda(c_1 + \sigma_f c_2) \\ \Lambda(c_1 + \sigma_f c_2) & M + \frac{(p_i + c_i^3)^2}{2M'} + \sigma_f \frac{(p_1 + c_1^3)(p_2 + c_2^3)}{M''} \end{pmatrix}. \quad (4.8)$$

The hole-one-magnon vertex proportional to Λ mixes the spin $s = +$ and $s = -$ states and provides a potential mechanism to stabilize a spiral phase. The diagonalization of the above Hamiltonian yields

$$E_{\pm}^f(\vec{p}) = M + \frac{p_i^2 + (c_i^3)^2}{2M'} + \sigma_f \frac{p_1 p_2 + c_1^3 c_2^3}{M''} \pm \sqrt{\left(\frac{p_i c_i^3}{M'} + \sigma_f \frac{p_1 c_2^3 + p_2 c_1^3}{M''} \right)^2 + \Lambda^2 (c_1 + \sigma_f c_2)^2}. \quad (4.9)$$

In particular, mixing via the Λ vertex lowers the energy E_-^f and raises the energy E_+^f . It should be noted that in this case the index \pm no longer refers to the spin orientation. Indeed, the eigenvectors corresponding to E_{\pm}^f are linear combinations of both spins. The minimum of the energy is located at $\vec{p} = 0$ for which

$$E_{\pm}^f(0) = M + \frac{(c_i^3)^2}{2M'} + \sigma_f \frac{c_1^3 c_2^3}{M''} \pm \Lambda |c_1 + \sigma_f c_2|. \quad (4.10)$$

Since c_i^3 does not affect the magnon contribution to the energy density, we fix it by minimizing $E_-^f(0)$ which implies $c_1^3 = c_2^3 = 0$. According to eq.(3.7) this implies that $\theta_0 = \frac{\pi}{2}$, i.e. the spiral is along a great circle on the sphere S^2 . By repeating the whole calculation including terms of $\mathcal{O}((c_i^3)^2)$, we have verified a posteriori that putting $c_i^3 = 0$ is indeed justified. At present we cannot exclude that there might be a minimum with a lower energy for large values of the c_i^3 . Investigating this issue would require a somewhat tedious numerical calculation which we have not yet performed. For $c_1^3 = c_2^3 = 0$ the energies of eq.(4.9) reduce to

$$E_{\pm}^f(\vec{p}) = M + \frac{p_i^2}{2M'} + \sigma_f \frac{p_1 p_2}{M''} \pm \Lambda |c_1 + \sigma_f c_2|. \quad (4.11)$$

Consequently, the filled hole pockets P_{\pm}^f (with $M' < M''$) are ellipses determined by

$$\frac{p_i^2}{2M'} + \sigma_f \frac{p_1 p_2}{M''} = T_{\pm}^f, \quad (4.12)$$

where T_{\pm}^f is the kinetic energy of a hole in the pocket P_{\pm}^f at the Fermi surface. The area of an occupied hole pocket determines the fermion density as

$$n_{\pm}^f = \frac{1}{(2\pi)^2} \int_{P_{\pm}^f} d^2 p = \frac{1}{2\pi} M_{\text{eff}} T_{\pm}^f, \quad M_{\text{eff}} = \frac{M' M''}{\sqrt{M''^2 - M'^2}}. \quad (4.13)$$

The kinetic energy density of a filled pocket is given by

$$t_{\pm}^f = \frac{1}{(2\pi)^2} \int_{P_{\pm}^f} d^2p \left(\frac{p_i^2}{2M'} + \sigma_f \frac{p_1 p_2}{M''} \right) = \frac{1}{4\pi} M_{\text{eff}} T_{\pm}^{f2}. \quad (4.14)$$

The total density of fermions of all flavors is

$$n = n_+^{\alpha} + n_-^{\alpha} + n_+^{\beta} + n_-^{\beta} = \frac{1}{2\pi} M_{\text{eff}} (T_+^{\alpha} + T_-^{\alpha} + T_+^{\beta} + T_-^{\beta}), \quad (4.15)$$

and the total energy density of the holes is

$$\epsilon_h = \epsilon_+^{\alpha} + \epsilon_-^{\alpha} + \epsilon_+^{\beta} + \epsilon_-^{\beta}, \quad (4.16)$$

with

$$\epsilon_{\pm}^f = (M \pm \Lambda |c_1 + \sigma_f c_2|) n_{\pm}^f + t_{\pm}^f. \quad (4.17)$$

The filling of the various hole pockets is controlled by the parameters T_{\pm}^f which must be varied in order to minimize the energy while keeping the total density of holes fixed. We thus introduce

$$S = \epsilon_h - \mu n, \quad (4.18)$$

where μ is a Lagrange multiplier that fixes the density, and we demand

$$\frac{\partial S}{\partial T_{\pm}^f} = \frac{1}{2\pi} M_{\text{eff}} (M \pm \Lambda |c_1 + \sigma_f c_2| + T_{\pm}^f - \mu) = 0. \quad (4.19)$$

One may wonder if the density of holes of flavor α and β should not be fixed separately. After all, flavor is conserved due to the accidental $U(1)_F$ symmetry. While the $U(1)_F$ symmetry arises for the leading terms in the effective action, it is not present at the microscopic level. Although they enter the effective theory only at higher orders, there are physical processes that can change flavor. Despite the fact that such processes are rare, it would hence be inappropriate to fix the fermion numbers of different flavors separately.

4.3 Four Populated Hole Pockets: Homogeneous Phase

We will now populate the various hole pockets with fermions. First, we keep the configuration of the staggered magnetization fixed and we vary the T_{\pm}^f in order to minimize the energy of the fermions. Then we also vary the parameters c_i of the magnon field in order to minimize the total energy. One must distinguish various cases, depending on how many hole pockets are populated with fermions. In this subsection, we consider the case of populating all four hole pockets (i.e. with both flavors $f = \alpha, \beta$ and with both energy indices \pm). In this case, eq.(4.19) implies

$$\mu = M + \frac{\pi n}{2M_{\text{eff}}}, \quad T_{\pm}^f = \frac{\pi n}{2M_{\text{eff}}} \mp \Lambda |c_1 + \sigma_f c_2|. \quad (4.20)$$

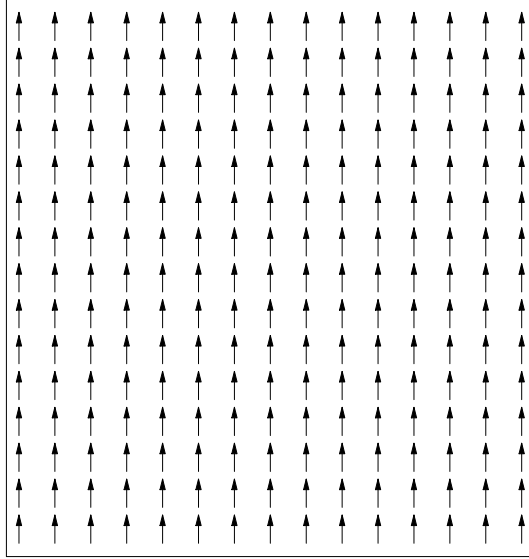


Figure 2: *The homogeneous phase with constant staggered magnetization.*

The total energy density then takes the form

$$\begin{aligned}
\epsilon &= \epsilon_0 + \epsilon_m + \epsilon_h = \epsilon_0 + 2\rho_s(c_1^2 + c_2^2) + \epsilon_+^\alpha + \epsilon_-^\alpha + \epsilon_+^\beta + \epsilon_-^\beta \\
&= \epsilon_0 + 2\rho_s(c_1^2 + c_2^2) + Mn + \frac{\pi n^2}{4M_{\text{eff}}} - \frac{1}{\pi}M_{\text{eff}}\Lambda^2(c_1^2 + c_2^2). \quad (4.21)
\end{aligned}$$

For $2\pi\rho_s > M_{\text{eff}}\Lambda^2$ the energy is minimized for $c_i = 0$ and the configuration is thus homogeneous. The total energy density in the four-pocket case is then given by

$$\epsilon_4 = \epsilon_0 + Mn + \frac{\pi n^2}{4M_{\text{eff}}}. \quad (4.22)$$

The homogeneous phase is shown in figure 2. For $2\pi\rho_s < M_{\text{eff}}\Lambda^2$, on the other hand, the energy is not bounded from below. In this case, $c_1^2 + c_2^2$ seems to grow without bound. However, according to eq.(4.20) this would lead to $T_+^f < 0$ which is physically meaningless. What really happens is that one pocket gets completely emptied and we must thus turn to the three-pocket case.

4.4 Three Populated Hole Pockets: 45 Degrees Spiral

We now populate only three pockets with holes: the two pockets with the lower energies E_-^α and E_-^β as well as the pocket with the higher energy E_+^α . Of course, alternatively one could also fill the β_+ -pocket. We now obtain

$$n = n_+^\alpha + n_-^\alpha + n_-^\beta = \frac{1}{2\pi}M_{\text{eff}}(T_+^\alpha + T_-^\alpha + T_-^\beta), \quad \epsilon_h = \epsilon_+^\alpha + \epsilon_-^\alpha + \epsilon_-^\beta, \quad (4.23)$$

such that eq.(4.19) yields

$$\begin{aligned}
\mu &= M + \frac{2\pi n}{3M_{\text{eff}}} - \frac{\Lambda}{3}|c_1 - c_2|, \\
T_+^\alpha &= \frac{2\pi n}{3M_{\text{eff}}} - \Lambda|c_1 + c_2| - \frac{\Lambda}{3}|c_1 - c_2|, \\
T_-^\alpha &= \frac{2\pi n}{3M_{\text{eff}}} + \Lambda|c_1 + c_2| - \frac{\Lambda}{3}|c_1 - c_2|, \\
T_-^\beta &= \frac{2\pi n}{3M_{\text{eff}}} + \frac{2\Lambda}{3}|c_1 - c_2|.
\end{aligned} \tag{4.24}$$

The total energy density then takes the form

$$\begin{aligned}
\epsilon &= \epsilon_0 + \epsilon_m + \epsilon_h = \epsilon_0 + 2\rho_s(c_1^2 + c_2^2) + \epsilon_+^\alpha + \epsilon_-^\alpha + \epsilon_-^\beta \\
&= \epsilon_0 + 2\rho_s(c_1^2 + c_2^2) + \left(M - \frac{\Lambda}{3}|c_1 - c_2|\right)n + \frac{\pi n^2}{3M_{\text{eff}}} \\
&\quad - \frac{2}{3\pi}M_{\text{eff}}\Lambda^2(c_1^2 + c_1c_2 + c_2^2).
\end{aligned} \tag{4.25}$$

For $2\pi\rho_s > M_{\text{eff}}\Lambda^2$ the energy density is bounded from below and its minimum is located at $c_1 = -c_2$ with

$$|c_1| = |c_2| = \frac{\pi}{2} \frac{\Lambda n}{6\pi\rho_s - M_{\text{eff}}\Lambda^2}. \tag{4.26}$$

This represents a spiral in the staggered magnetization oriented along a lattice diagonal — a 45 degrees spiral. When one occupies the β_+ - instead of the α_+ -pocket, one finds $c_1 = c_2$, i.e. the spiral is then oriented in the orthogonal diagonal direction. According to eq.(A.19) in the appendix, the spiral pitch (i.e. the wave number of the spiral) is given by

$$k = 2\sqrt{c_i^3c_i^3 + c_i c_i} = 2\sqrt{c_1^2 + c_2^2} = \frac{\sqrt{2}\pi\Lambda n}{6\pi\rho_s - M_{\text{eff}}\Lambda^2}. \tag{4.27}$$

The resulting energy density in the three-pocket case takes the form

$$\epsilon_3 = \epsilon_0 + Mn + \frac{\pi}{3M_{\text{eff}}} \left(1 - \frac{1}{2} \frac{M_{\text{eff}}\Lambda^2}{6\pi\rho_s - M_{\text{eff}}\Lambda^2}\right) n^2. \tag{4.28}$$

The 45 degrees spiral is illustrated in figure 3. It is energetically less favorable than the homogeneous phase because $\epsilon_3 > \epsilon_4$ for $2\pi\rho_s > M_{\text{eff}}\Lambda^2$. Only for $2\pi\rho_s = M_{\text{eff}}\Lambda^2$ both phases cost the same energy, i.e. $\epsilon_3 = \epsilon_4$. For $2\pi\rho_s < M_{\text{eff}}\Lambda^2$ the energy density of eq.(4.25) is unbounded from below and $c_1^2 + c_2^2$ again seems to grow without bound. This, however, would lead to $T_+^\alpha < 0$ which is unphysical. In fact, the α_+ -pocket is completely emptied and we are thus led to investigate the two-pocket case.

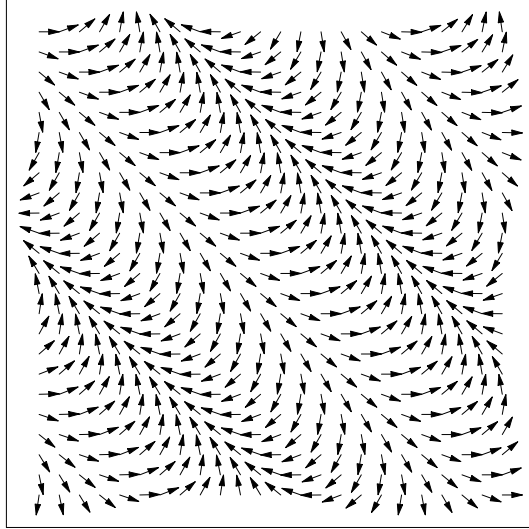


Figure 3: A 45 degrees spiral oriented along a lattice diagonal.

4.5 Two Populated Hole Pockets: Zero Degree Spiral

We now populate only two pockets with holes. These are necessarily the pockets with the lower energies E_-^α and E_-^β . In this case we have

$$n = n_-^\alpha + n_-^\beta = \frac{1}{2\pi} M_{\text{eff}} (T_-^\alpha + T_-^\beta), \quad \epsilon_h = \epsilon_-^\alpha + \epsilon_-^\beta, \quad (4.29)$$

and thus eq.(4.19) now implies

$$\begin{aligned} \mu &= M + \frac{\pi n}{M_{\text{eff}}} - \frac{\Lambda}{2} (|c_1 + c_2| + |c_1 - c_2|), \\ T_-^\alpha &= \frac{\pi n}{M_{\text{eff}}} + \frac{\Lambda}{2} (|c_1 + c_2| - |c_1 - c_2|), \\ T_-^\beta &= \frac{\pi n}{M_{\text{eff}}} + \frac{\Lambda}{2} (|c_1 - c_2| - |c_1 + c_2|). \end{aligned} \quad (4.30)$$

The total energy density then takes the form

$$\begin{aligned} \epsilon &= \epsilon_0 + \epsilon_m + \epsilon_h = \epsilon_0 + 2\rho_s (c_1^2 + c_2^2) + \epsilon_-^\alpha + \epsilon_-^\beta \\ &= \epsilon_0 + 2\rho_s (c_1^2 + c_2^2) + \left(M - \frac{\Lambda}{2} (|c_1 + c_2| + |c_1 - c_2|) \right) n + \frac{\pi n^2}{2M_{\text{eff}}} \\ &\quad - \frac{1}{2\pi} M_{\text{eff}} \frac{\Lambda^2}{4} (|c_1 + c_2| - |c_1 - c_2|)^2. \end{aligned} \quad (4.31)$$

For $2\pi\rho_s > \frac{1}{2}M_{\text{eff}}\Lambda^2$ the energy density is bounded from below and has its minimum at

$$|c_1| = \frac{\Lambda}{4\rho_s} n, \quad |c_2| = 0, \quad \text{or} \quad |c_1| = 0, \quad |c_2| = \frac{\Lambda}{4\rho_s} n, \quad (4.32)$$

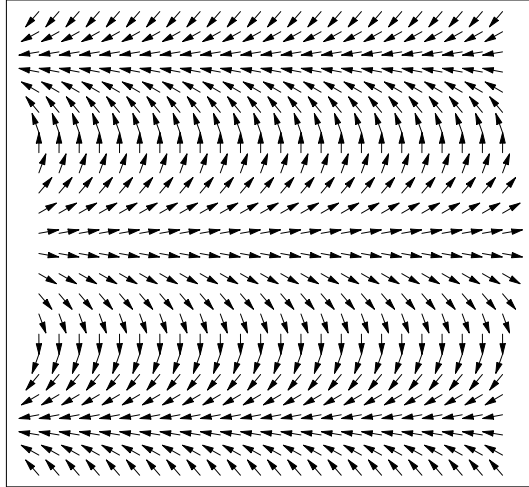


Figure 4: *A zero degree spiral oriented along a lattice axis.*

which corresponds to a spiral in the staggered magnetization oriented along a lattice axis — a zero degree spiral. Again, according to eq.(A.19), the wave number of the spiral is given by

$$k = 2\sqrt{c_i^3 c_i^3 + c_i c_i} = 2\sqrt{c_1^2 + c_2^2} = \frac{\Lambda n}{2\rho_s}, \quad (4.33)$$

and the resulting energy density in the two-pocket case takes the form

$$\epsilon_2 = \epsilon_0 + Mn + \left(\frac{\pi}{2M_{\text{eff}}} - \frac{\Lambda^2}{8\rho_s} \right) n^2. \quad (4.34)$$

The zero degree spiral is more stable than the homogeneous phase if $\epsilon_2 < \epsilon_4$, which is the case for $2\pi\rho_s < M_{\text{eff}}\Lambda^2$. This also clarifies the instability of the homogeneous phase in this parameter regime: it simply turns into the zero degree spiral. We have verified explicitly that the assumption $c_i^3 = 0$ is justified by repeating the whole calculation including terms up to $\mathcal{O}((c_i^3)^2)$. Indeed, $c_i^3 = 0$ turns out to be a stable minimum for $2\pi\rho_s < M_{\text{eff}}\Lambda^2$. The zero degree spiral is illustrated in figure 4.

4.6 One Populated Hole Pocket: 45 Degrees Spiral

Finally, let us populate only one hole pocket, say the states with energy E_-^α . Of course, alternatively one could also occupy the β_- -pocket. One now obtains

$$T_-^\alpha = \frac{2\pi n}{M_{\text{eff}}}. \quad (4.35)$$

The total energy density then takes the form

$$\begin{aligned}\epsilon &= \epsilon_0 + \epsilon_m + \epsilon_h = \epsilon_0 + 2\rho_s(c_1^2 + c_2^2) + \epsilon_- \\ &= \epsilon_0 + 2\rho_s(c_1^2 + c_2^2) + (M - \Lambda|c_1 + c_2|)n + \frac{\pi n^2}{M_{\text{eff}}},\end{aligned}\quad (4.36)$$

which is minimized for $c_1 = c_2$ with

$$|c_1| = |c_2| = \frac{\Lambda}{4\rho_s}n. \quad (4.37)$$

This again represents a 45 degrees spiral in the staggered magnetization oriented along a lattice diagonal. When one occupies the β_- -pocket one finds $c_1 = -c_2$, i.e., as in the three-pocket case, the α - and β -spirals are oriented in orthogonal diagonal directions. Note that the three-pocket 45 degrees spiral with an occupied α_+ -pocket is oriented in a direction orthogonal to the one of the one-pocket 45 degrees spiral with an occupied α_- -pocket. In the one-pocket case, the spiral pitch is given by

$$k = 2\sqrt{c_i^3 c_i^3 + c_i c_i} = 2\sqrt{c_1^2 + c_2^2} = \frac{\Lambda n}{\sqrt{2\rho_s}}, \quad (4.38)$$

and the corresponding energy density takes the form

$$\epsilon_1 = \epsilon_0 + Mn + \left(\frac{\pi}{M_{\text{eff}}} - \frac{\Lambda^2}{4\rho_s} \right) n^2. \quad (4.39)$$

The 45 degrees spiral is energetically more favorable than the zero degree spiral if $\epsilon_1 < \epsilon_2$, which is the case for $2\pi\rho_s < \frac{1}{2}M_{\text{eff}}\Lambda^2$. Again, by repeating the whole calculation including terms up to $\mathcal{O}((c_i^3)^2)$, we have verified explicitly that for $2\pi\rho_s < M_{\text{eff}}\Lambda^2$ the assumption of $c_i^3 = 0$ is justified because it corresponds to a stable minimum.

However, as already pointed out in [24, 27, 36, 42, 43], the negative coefficient of the term proportional to n^2 (i.e. a negative compressibility) leads to an instability of the 45 degrees spiral against increasing the local fermion density by decreasing the wavelength $2\pi/k$ of the spiral. To see this, let us consider a one-pocket 45 degrees spiral filling a sub-volume V' and leaving an undoped antiferromagnet behind in the remaining volume $V - V'$. The energy density of this configuration with an inhomogeneous fermion density is given by

$$\begin{aligned}\epsilon_{\text{inh}} &= \epsilon_1 \frac{V'}{V} + \epsilon_0 \frac{V - V'}{V} = \epsilon_0 + \left[Mn + \left(\frac{\pi}{M_{\text{eff}}} - \frac{\Lambda^2}{4\rho_s} \right) n^2 \right] \frac{V'}{V} \\ &= \epsilon_0 + \left[M \frac{N}{V'} + \left(\frac{\pi}{M_{\text{eff}}} - \frac{\Lambda^2}{4\rho_s} \right) \left(\frac{N}{V'} \right)^2 \right] \frac{V'}{V} \\ &= \epsilon_0 + \left[M + \left(\frac{\pi}{M_{\text{eff}}} - \frac{\Lambda^2}{4\rho_s} \right) \frac{N}{V'} \right] \frac{N}{V}.\end{aligned}\quad (4.40)$$

Since the coefficient of the term proportional to $1/V'$ is negative for $2\pi\rho_s < \frac{1}{2}M_{\text{eff}}\Lambda^2$, the system can minimize its energy by shrinking V' and thus increasing the fermion density n in the region of the 45 degrees spiral. The one-pocket 45 degrees spiral is thus unstable against the formation of inhomogeneities in the fermion density. Our basic assumption that the system is homogeneous is then not satisfied.

4.7 Symmetry Breaking Pattern in the Spiral Phase

As we have seen, for intermediate values of ρ_s a spiral phase replaces the phase with homogeneous staggered magnetization. In the homogeneous phase the $SU(2)_s$ spin symmetry is spontaneously broken to its $U(1)_s$ subgroup. Due to antiferromagnetism, the displacement by one lattice spacing is also spontaneously broken. In a spiral phase, on the other hand, a $U(1)_s$ spin rotation that leaves the configuration invariant no longer exists. Hence, $U(1)_s$ is then also spontaneously broken and one may expect an additional massless Goldstone boson. Furthermore, due to the finite wavelength $2\pi/k$ of the spiral, translation invariance (not only by one lattice spacing) is also spontaneously broken. Only the translations by an integer multiple of the spiral wavelength remain unbroken. Due to the spontaneously broken translation symmetry one expects yet another massless Goldstone boson — a spiral phonon (or helimagnon) — which corresponds to vibrations of the spiral. In order to correctly count the number of Goldstone bosons one must notice that while both $U(1)_s$ and translation invariance are individually spontaneously broken, there is a combination of these two symmetries that remains unbroken. In particular, any translation of the spiral configuration can be compensated by an appropriate $U(1)_s$ spin rotation. Consequently, there are not two but there is only one additional Goldstone boson — the spiral phonon. Besides this additional massless boson, in the spiral configuration there are still two magnons — a transverse and a longitudinal one. The transverse magnon corresponds to spin fluctuations out of the spiral plane, while the longitudinal magnon represents in-plane fluctuations.

It should be noted that the wavelength $2\pi/k \propto 1/n$ of the spiral represents a new length scale in the problem. In particular, for very small fermion density n this length scale is arbitrarily long. In that case, the spiral phonon will have very little effect on the dynamics of the holes. When the fermion density increases, the spiral wavelength shrinks and the spiral phonon becomes more important. In particular, besides magnon exchange the exchange of spiral phonons may then contribute significantly to the long-range interactions between the holes.

Since the symmetry is no longer broken just from $SU(2)_s$ to $U(1)_s$, one may wonder whether the vector $\vec{e}(x)$ living in the coset space $SU(2)_s/U(1)_s = S^2$ is still an appropriate low-energy degree of freedom in the spiral phase. Fortunately, this is indeed the case. Since the spiral phonon arises as an additional Goldstone boson, one may also wonder whether a new field must be added to the effective Lagrangian.

This is not necessary because, just like the two magnons, the spiral phonon arises as a fluctuation of the staggered magnetization vector $\vec{e}(x)$ (in this case around the spiral configuration). Only if one would construct another effective theory valid only at extremely long length scales much larger than the wavelength of the spiral, the basic fields of the theory would have to be redefined. In such an effective theory the spiral itself would be a short distance phenomenon and the spiral phonon would appear explicitly as an independent degree of freedom. The corresponding physics at extremely low energies is still contained in our effective theory which is valid at length scales both longer and shorter than the wavelength of the spiral.

5 Inclusion of 4-Fermion Couplings in Perturbation Theory

In this section the 4-fermion contact interactions are incorporated in perturbation theory. Depending on the microscopic system in question, the 4-fermion couplings may or may not be small. If they are large, the result of the perturbative calculation should not be trusted. In that case, one could still perform a variational calculation. In this work we limit ourselves to first order perturbation theory. We will distinguish four cases: the homogeneous phase, the three-pocket 45 degrees spiral, the zero degree spiral, and the one-pocket 45 degrees spiral. Finally, depending on the values of the low-energy constants, we determine which phase is energetically favorable.

5.1 Four-Pocket Case: Homogeneous Phase

Let us first consider the homogeneous phase. The perturbation of the Hamiltonian due to the leading 4-fermion contact terms of eq.(2.18) is given by

$$\begin{aligned} \Delta H = \int d^2x \sum_{s=+,-} & \left[\frac{G_1}{2} (\Psi_s^{\alpha\dagger} \Psi_s^\alpha \Psi_{-s}^{\alpha\dagger} \Psi_{-s}^\alpha + \Psi_s^{\beta\dagger} \Psi_s^\beta \Psi_{-s}^{\beta\dagger} \Psi_{-s}^\beta) \right. \\ & \left. + G_2 \Psi_s^{\alpha\dagger} \Psi_s^\alpha \Psi_s^{\beta\dagger} \Psi_s^\beta + G_3 \Psi_s^{\alpha\dagger} \Psi_s^\alpha \Psi_{-s}^{\beta\dagger} \Psi_{-s}^\beta \right]. \end{aligned} \quad (5.1)$$

It should be noted that $\Psi_s^{f\dagger}(x)$ and $\Psi_s^f(x)$ again are fermion creation and annihilation operators (and not Grassmann numbers). The term proportional to G_4 is of higher order and hence need not be considered here. In the homogeneous phase the fermion density is equally distributed among the two spin orientations and the two flavors such that

$$\langle \Psi_+^{\alpha\dagger} \Psi_+^\alpha \rangle = \langle \Psi_-^{\alpha\dagger} \Psi_-^\alpha \rangle = \langle \Psi_+^{\beta\dagger} \Psi_+^\beta \rangle = \langle \Psi_-^{\beta\dagger} \Psi_-^\beta \rangle = \frac{n}{4}. \quad (5.2)$$

The brackets denote expectation values in the unperturbed state determined in section 4.3. Since the fermions are uncorrelated, for $f \neq f'$ or $s \neq s'$ one has

$$\langle \Psi_s^{f\dagger} \Psi_s^f \Psi_{s'}^{f'\dagger} \Psi_{s'}^{f'} \rangle = \langle \Psi_s^{f\dagger} \Psi_s^f \rangle \langle \Psi_{s'}^{f'\dagger} \Psi_{s'}^{f'} \rangle. \quad (5.3)$$

Taking the 4-fermion contact terms into account in first order perturbation theory, the total energy density of eq.(4.22) receives an additional contribution and now reads

$$\epsilon_4 = \epsilon_0 + Mn + \frac{\pi n^2}{4M_{\text{eff}}} + \frac{1}{8}(G_1 + G_2 + G_3)n^2. \quad (5.4)$$

5.2 Three-Pocket Case: 45 Degrees Spiral

For $c_i^3 = 0$ the eigenvectors of the single-particle Hamiltonian of eq.(4.8) corresponding to the energy eigenvalues $E_{\pm}^f(\vec{p})$ are given by

$$\tilde{\Psi}_{\pm}^f = \frac{1}{\sqrt{2}}(\Psi_{-}^f \pm \Psi_{+}^f) \Rightarrow \Psi_{\pm}^f = \frac{1}{\sqrt{2}}(\tilde{\Psi}_{+}^f \mp \tilde{\Psi}_{-}^f). \quad (5.5)$$

Inserting this expression in eq.(5.1) allows us to evaluate the expectation value $\langle \Delta H \rangle$ in the unperturbed states determined in section 4. In the three-pocket case the states with energies $E_{-}^{\alpha}(\vec{p})$, $E_{-}^{\beta}(\vec{p})$, as well as $E_{+}^{\alpha}(\vec{p})$ (or alternatively $E_{+}^{\beta}(\vec{p})$), and with \vec{p} inside the respective hole pocket are occupied and

$$\begin{aligned} \langle \tilde{\Psi}_{+}^{\alpha\dagger} \tilde{\Psi}_{+}^{\alpha} \rangle &= \langle \tilde{\Psi}_{-}^{\alpha\dagger} \tilde{\Psi}_{-}^{\alpha} \rangle = \left(1 - \frac{1}{2} \frac{M_{\text{eff}}\Lambda^2}{6\pi\rho_s - M_{\text{eff}}\Lambda^2} \right) \frac{n}{3}, \\ \langle \tilde{\Psi}_{-}^{\beta\dagger} \tilde{\Psi}_{-}^{\beta} \rangle &= \left(1 + \frac{M_{\text{eff}}\Lambda^2}{6\pi\rho_s - M_{\text{eff}}\Lambda^2} \right) \frac{n}{3}, \quad \langle \tilde{\Psi}_{+}^{\beta\dagger} \tilde{\Psi}_{+}^{\beta} \rangle = 0. \end{aligned} \quad (5.6)$$

As a result the energy density of eq.(4.28) turns into

$$\begin{aligned} \epsilon_3 &= \epsilon_0 + Mn + \frac{\pi}{3M_{\text{eff}}} \left(1 - \frac{1}{2} \frac{M_{\text{eff}}\Lambda^2}{6\pi\rho_s - M_{\text{eff}}\Lambda^2} \right) n^2 \\ &+ \frac{1}{4} [(G_1 + G_2 + G_3)4\pi\rho_s - G_1 M_{\text{eff}}\Lambda^2] \frac{4\pi\rho_s - M_{\text{eff}}\Lambda^2}{(6\pi\rho_s - M_{\text{eff}}\Lambda^2)^2} n^2. \end{aligned} \quad (5.7)$$

5.3 Two-Pocket Case: Zero Degree Spiral

In the zero degree spiral only the states with energy $E_{-}^{\alpha}(\vec{p})$ and $E_{-}^{\beta}(\vec{p})$ with \vec{p} inside the respective hole pocket P_{-}^f are occupied and hence

$$\langle \tilde{\Psi}_{-}^{\alpha\dagger} \tilde{\Psi}_{-}^{\alpha} \rangle = \langle \tilde{\Psi}_{-}^{\beta\dagger} \tilde{\Psi}_{-}^{\beta} \rangle = \frac{n}{2}, \quad \langle \tilde{\Psi}_{+}^{\alpha\dagger} \tilde{\Psi}_{+}^{\alpha} \rangle = \langle \tilde{\Psi}_{+}^{\beta\dagger} \tilde{\Psi}_{+}^{\beta} \rangle = 0. \quad (5.8)$$

As a result the energy density of eq.(4.34) turns into

$$\epsilon_2 = \epsilon_0 + Mn + \left(\frac{\pi}{2M_{\text{eff}}} - \frac{\Lambda^2}{8\rho_s} \right) n^2 + \frac{1}{8}(G_2 + G_3)n^2. \quad (5.9)$$

5.4 One-Pocket Case: 45 Degrees Spiral

In the one-pocket case only the states with energy $E_-^\alpha(\vec{p})$ (or alternatively with $E_-^\beta(\vec{p})$) and with \vec{p} inside the corresponding hole pocket are occupied such that

$$\langle \tilde{\Psi}_-^{\alpha\dagger} \tilde{\Psi}_-^\alpha \rangle = n, \quad \langle \tilde{\Psi}_+^{\alpha\dagger} \tilde{\Psi}_+^\alpha \rangle = \langle \tilde{\Psi}_+^{\beta\dagger} \tilde{\Psi}_+^\beta \rangle = \langle \tilde{\Psi}_-^{\beta\dagger} \tilde{\Psi}_-^\beta \rangle = 0. \quad (5.10)$$

In this case the 4-fermion terms do not contribute to the energy density which thus maintains the form of eq.(4.39), i.e.

$$\epsilon_1 = \epsilon_0 + Mn + \left(\frac{\pi}{M_{\text{eff}}} - \frac{\Lambda^2}{4\rho_s} \right) n^2. \quad (5.11)$$

5.5 Stability Ranges of Various Phases

Let us summarize the results of the previous subsections. The energy densities of the various phases take the form

$$\epsilon_i = \epsilon_0 + Mn + \frac{1}{2} \kappa_i n^2. \quad (5.12)$$

According to eqs.(5.11), (5.9), (5.7), and (5.4), the compressibilities are given by

$$\begin{aligned} \kappa_1 &= \frac{2\pi}{M_{\text{eff}}} - \frac{\Lambda^2}{2\rho_s}, \\ \kappa_2 &= \frac{\pi}{M_{\text{eff}}} - \frac{\Lambda^2}{4\rho_s} + \frac{1}{4}(G_2 + G_3), \\ \kappa_3 &= \frac{2\pi}{3M_{\text{eff}}} \left(1 - \frac{1}{2} \frac{M_{\text{eff}}\Lambda^2}{6\pi\rho_s - M_{\text{eff}}\Lambda^2} \right) \\ &\quad + \frac{1}{2} \left[(G_1 + G_2 + G_3)4\pi\rho_s - G_1 M_{\text{eff}}\Lambda^2 \right] \frac{4\pi\rho_s - M_{\text{eff}}\Lambda^2}{(6\pi\rho_s - M_{\text{eff}}\Lambda^2)^2}, \\ \kappa_4 &= \frac{\pi}{2M_{\text{eff}}} + \frac{1}{4}(G_1 + G_2 + G_3). \end{aligned} \quad (5.13)$$

The compressibilities κ_i as functions of $M_{\text{eff}}\Lambda^2/2\pi\rho_s$ are shown in figure 5. For large values of ρ_s , spiral phases cost a large amount of magnetic energy and a homogeneous phase is more stable. The energy density of the homogeneous phase is lower than the one of the spiral phases for $\kappa_4 < \kappa_1, \kappa_2, \kappa_3$, which is the case for

$$M_{\text{eff}}\Lambda^2 + G_1 \frac{M_{\text{eff}}^2\Lambda^2}{2\pi} \leq 2\pi\rho_s \quad \begin{cases} \text{Four-pocket case:} \\ \text{Homogeneous phase.} \end{cases} \quad (5.14)$$

At $\mathcal{O}(G_i)$ the three-pocket 45 degrees spiral always costs more energy than the other phases, except at the specific point

$$2\pi\rho_s = M_{\text{eff}}\Lambda^2 + G_1 \frac{M_{\text{eff}}^2\Lambda^2}{2\pi} \quad \begin{cases} \text{Three-pocket case:} \\ \text{45 degrees spiral.} \end{cases} \quad (5.15)$$

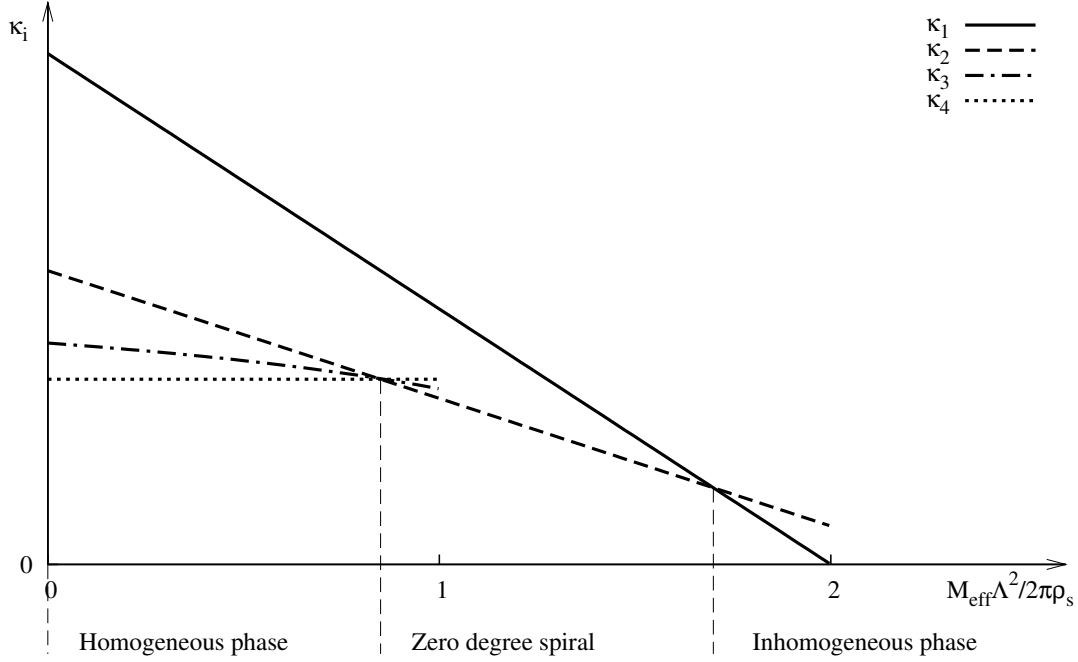


Figure 5: The compressibilities κ_i (in the presence of weak repulsive 4-fermion couplings) as functions of $M_{\text{eff}}\Lambda^2/2\pi\rho_s$ determine the stability ranges of the various phases. A homogeneous phase, a zero degree spiral, or an inhomogeneous phase are energetically favorable, for large, intermediate, and small values of ρ_s , respectively. Only at the two isolated points separating the three regimes a 45 degrees spiral, either with one or with three populated hole pockets, is degenerate with the other phases. The three- and four-pocket cases become unstable at $M_{\text{eff}}\Lambda^2/2\pi\rho_s = 1$, and the one- and two-pocket cases become unstable at $M_{\text{eff}}\Lambda^2/2\pi\rho_s = 2$.

For this particular value of ρ_s the three-pocket 45 degrees spiral costs the same energy as the homogeneous phase and the zero degree spiral. For larger values of the 4-fermion couplings (not accessible to first order perturbation theory) it is conceivable that the 45 degrees spiral becomes energetically favorable. This could be investigated, for example, using a variational calculation. For intermediate values of ρ_s the homogeneous phase becomes unstable against the formation of a zero degree spiral, i.e. $\kappa_2 < \kappa_4$, and we find

$$\frac{1}{2}M_{\text{eff}}\Lambda^2 + (G_2 + G_3)\frac{M_{\text{eff}}^2\Lambda^2}{8\pi} \leq 2\pi\rho_s \leq M_{\text{eff}}\Lambda^2 + G_1\frac{M_{\text{eff}}^2\Lambda^2}{2\pi} \begin{cases} \text{Two-pocket case:} \\ \text{Zero degree spiral.} \end{cases} \quad (5.16)$$

For smaller values of ρ_s the one-pocket 45 degrees spiral becomes energetically more favorable than the zero degree spiral, i.e. $\kappa_1 < \kappa_2$, but the one-pocket 45 degrees spiral exists only at the isolated point

$$2\pi\rho_s = \frac{1}{2}M_{\text{eff}}\Lambda^2 + (G_2 + G_3)\frac{M_{\text{eff}}^2\Lambda^2}{8\pi} \begin{cases} \text{One-pocket case:} \\ \text{45 degrees spiral.} \end{cases} \quad (5.17)$$

It may seem that a repulsive 4-fermion interaction $G_2 + G_3 > 0$ stabilizes the 45 degrees spiral, at least in the narrow parameter range down to $2\pi\rho_s = \frac{1}{2}M_{\text{eff}}\Lambda^2$. However, although we have not yet identified the nature of the inhomogeneous phase, we expect that it will be energetically more favorable, such that

$$2\pi\rho_s \leq \frac{1}{2}M_{\text{eff}}\Lambda^2 + (G_2 + G_3)\frac{M_{\text{eff}}^2\Lambda^2}{8\pi} \left\{ \begin{array}{l} \text{Inhomogeneous phase of} \\ \text{yet unidentified nature.} \end{array} \right. \quad (5.18)$$

At least at $\mathcal{O}(G_i)$, the 45 degrees spiral cannot be realized in this regime, because for $G_i = 0$ it only exists at the isolated point $2\pi\rho_s = \frac{1}{2}M_{\text{eff}}\Lambda^2$ and first order perturbation theory uses just the unperturbed wave function. Definitely, the one-pocket 45 degrees spiral becomes unstable when $\kappa_1 < 0$, i.e. for

$$2\pi\rho_s \leq \frac{1}{2}M_{\text{eff}}\Lambda^2 \left\{ \begin{array}{l} \text{Instability of the 45 degrees spiral} \\ \text{against formation of inhomogeneities.} \end{array} \right. \quad (5.19)$$

It should be pointed out again that these results apply only if the 4-fermion contact interactions are weak. If the 4-fermion couplings are strong, the approach of filling pockets with weakly interacting holes is not applicable and the true ground state of the system may be different. Even if the 4-fermion couplings are small, the present result does not necessarily reveal the complete nature of the true ground state. In particular, the configurations of the staggered magnetization were restricted to those that imply a homogeneous composite vector field $v_i(x)'$, i.e. to spirals or to configurations that are homogeneous themselves. For example, the double spiral, which implies an inhomogeneous $v_i(x)'$, was not taken into account. Hence, we cannot exclude that the phases that we found may still be unstable against developing inhomogeneities, at least in certain parameter regions. This shall be explored in the future.

6 Reduction of the Staggered Magnetization upon Doping

Until now we have considered the Lagrangian or the Hamiltonian of the effective theory. Now we will see that other quantities can be constructed in a similar way. An observable of particular interest is the staggered magnetization which is the order parameter for the spontaneous breakdown of the $SU(2)_s$ symmetry. As the antiferromagnet is doped, the staggered magnetization is reduced until the $SU(2)_s$ symmetry is restored. In the actual materials this happens at relatively small doping, before high-temperature superconductivity sets in.

In the undoped antiferromagnet the local staggered magnetization is given by $\vec{M}_s(x) = \mathcal{M}_s\vec{e}(x)$. The low-energy parameter \mathcal{M}_s is the length of the staggered magnetization vector. For the Heisenberg model (or equivalently for the t - J model

at half-filling) this parameter has been determined with high precision in quantum Monte Carlo simulations resulting in $\mathcal{M}_s = 0.3074(2)/a^2$ [77, 78]. In a doped antiferromagnet the staggered magnetization receives additional contributions from the fermions such that

$$\vec{M}_s(x) = \left[\mathcal{M}_s - m \sum_{\substack{f=\alpha,\beta \\ s=+,-}} \psi_s^{f\dagger}(x) \psi_s^f(x) \right] \vec{e}(x). \quad (6.1)$$

Here m is another low-energy parameter which determines the reduction of the staggered magnetization upon doping. It should be noted that there are further contributions to $\vec{M}_s(x)$ which include derivatives or contain more than two fermion fields. All these terms are of higher order and will be neglected here. Since both the homogeneous and the spiral phases have a constant fermion density we can use

$$\sum_{\substack{f=\alpha,\beta \\ s=+,-}} \langle \Psi_s^{f\dagger} \Psi_s^f \rangle = n, \quad (6.2)$$

such that

$$\mathcal{M}_s(n) = \mathcal{M}_s - mn. \quad (6.3)$$

The higher-order terms that we have neglected correct this equation at $\mathcal{O}(n^2)$. A rough estimate of the critical density at which the $SU(2)_s$ symmetry gets restored is $n_c \approx \mathcal{M}_s/m$. It would be interesting to determine the value of m for the t - J model, which may be feasible in quantum Monte Carlo calculations.

7 Conclusions and Outlook

In this paper we have used a systematic effective field theory for antiferromagnetic magnons and holes in order to investigate the propagation of holes in the background of a staggered magnetization field. We have limited ourselves to configurations of the staggered magnetization that are either homogeneous themselves or that generate a constant composite vector field $v_i(x)'$ for the fermions. In both cases, the resulting fermion density is homogeneous. Our calculations also rely on the assumption that remnant 4-fermion contact interactions between the holes are weak and can be treated in perturbation theory. This may or may not be the case for a concrete magnetic material. We like to emphasize again that the effective theory is universal and makes model-independent predictions for a large class of magnetic systems. Material-specific properties enter the effective theory through the values of low-energy parameters such as the spin stiffness ρ_s . For large values of ρ_s distortions in the staggered magnetization cost a large amount of energy and a homogeneous phase is energetically favored. In that case, all four hole pockets are equally populated with doped holes. For smaller values of ρ_s , on the other hand, the doped holes can gain energy from a spiral in the staggered magnetization. For intermediate values of ρ_s a zero degree spiral, in which only two hole pockets are populated,

is most stable, while a 45 degrees spiral (with either one or three populated hole pockets) can exist only at two specific isolated values of ρ_s . It is conceivable that the 45 degrees spirals may be stabilized for larger values of the 4-fermion couplings G_i (inaccessible to first order perturbation theory). For small values of ρ_s a yet unidentified inhomogeneous phase is energetically favored. The reduction of the staggered magnetization upon doping is again controlled by a low-energy parameter m whose value depends on the material in question.

The results of our investigation provide a basis for further studies that naturally suggest themselves. First, it would be interesting to investigate if there is a stable minimum of the energy for large values of c_i^3 . This requires a straightforward but somewhat tedious numerical calculation which we have not yet performed. Next, instead of using first order perturbation theory, one may want to include the 4-fermion couplings in a variational calculation. This would eliminate the assumption that these couplings are small. One should also analyze the stability of the homogeneous and spiral phases against developing inhomogeneities in the fermion density. For example, it is interesting to ask if a double spiral is energetically more favorable than the spiral phases considered here. If this were the case, it is conceivable that a lightly doped antiferromagnet without impurities is an insulator. The real materials are indeed insulators, but they contain impurities on which the doped holes may get localized.

On the other hand, if the homogeneous phase or the simple spirals considered here turn out to be more stable than, for example, a double spiral, the effects of magnon exchange between doped holes would be interesting to study in detail. In particular, using the effective theory, we have shown that the one-magnon exchange potential between two isolated holes gives rise to binding with d -wave characteristics [71, 76]. In a spiral phase the exchange of spiral phonons (i.e. helimagnons) may also be an important dynamical mechanism for the binding of hole pairs. Depending on the size of the pairs and on their density, hole pair formation may lead to Bose-Einstein condensation or to magnon-mediated BCS-type superconductivity coexisting with antiferromagnetism. While coexistence of superconductivity and antiferromagnetism is not observed in the high- T_c cuprates, this may be due to impurities created by doping on which holes may get localized, thus preventing superconductivity. A clean system like the t - J model, on the other hand, may superconduct already at small doping within the antiferromagnetic phase, although T_c may then be rather small. The effective theory provides us with a tool that allows us to address such questions. If there is superconductivity already within the antiferromagnetic phase in a clean system, the corresponding mechanism responsible for superconductivity may persist in the high- T_c cuprates, despite the fact that in the real materials at small doping superconductivity may be prevented by the localization of holes on impurities. Of course, once antiferromagnetism is destroyed, magnons and spiral phonons no longer exist as massless excitations. However, antiferromagnetic correlations, although only of finite range, still exist in high- T_c superconductors and may still play an important

role as relevant low-energy degrees of freedom. This is similar to nuclear physics where the pion is not exactly massless (in that case due to explicit chiral symmetry breaking) but is certainly relevant at low energies. Still, whether magnon-mediated binding between holes may be responsible for high-temperature superconductivity remains a difficult question that may or may not be within the applicability range of the effective theory. For lightly doped cuprates the low-energy effective field theory is applicable. It yields reliable and interesting results and should be pursued further.

Acknowledgements

C. P. H. would like to thank the members of the Institute for Theoretical Physics at Bern University for their hospitality during a visit at which this project was initiated. U.-J. W. likes to thank P. A. Lee for interesting discussions and the members of the Center for Theoretical Physics at MIT, where this work was completed, for their hospitality. This work was supported in part by funds provided by the Schweizerischer Nationalfonds. The work of C. P. H. is supported by CONACYT grant No. 50744-F, by Fondo Ramón Alvarez-Buylla de Aldana grant No. 349/05, and by grant PIFI 3.2.

A Most General Configuration with a Homogeneous Composite Vector Field

In this appendix we show that the most general configuration with constant $v_i(x)'$ corresponds to a spiral in the staggered magnetization. According to eq.(3.1) we need to consider $\theta(x)$, $\varphi(x)$, and $\alpha(x)$ such that

$$\begin{aligned} v_i^3(x)' &= v_i^3(x) - \partial_i \alpha(x) = \sin^2 \frac{\theta(x)}{2} \partial_i \varphi(x) - \partial_i \alpha(x) = c_i^3, \\ v_i^\pm(x)' &= v_i^\pm(x) \exp(\pm 2i\alpha(x)) \\ &= \frac{1}{2} (\sin \theta(x) \partial_i \varphi(x) \pm i \partial_i \theta(x)) \exp(\mp i(\varphi(x) - 2\alpha(x))) = c_i^\pm, \end{aligned} \quad (\text{A.1})$$

with c_i^\pm and c_i^3 being constant. Introducing $\chi(x) = \varphi(x) - 2\alpha(x)$ one obtains

$$\begin{aligned} \cos \theta(x) \partial_i \alpha(x) &= \sin^2 \frac{\theta(x)}{2} \partial_i \chi(x) - c_i^3, \\ \tan \theta(x) (\partial_i \chi(x) - 2c_i^3) \pm i \partial_i \theta(x) &= 2c_i^\pm \exp(\pm i\chi(x)) = 2c_i \exp(\pm i(\chi(x) + \omega_i)). \end{aligned} \quad (\text{A.2})$$

Here we have put

$$c_i^\pm = c_i \exp(\pm i\omega_i), \quad \text{with } c_i \in \mathbb{R}, \quad \omega_i \in \left[-\frac{\pi}{2}, \frac{\pi}{2}\right]. \quad (\text{A.3})$$

By an appropriate constant gauge transformation, one can always put $\omega_1 = 0$. From eq.(A.2) one infers

$$\begin{aligned}\tan \theta(x)(\partial_i \chi(x) - 2c_i^3) &= 2c_i \cos(\chi(x) + \omega_i), \\ \partial_i \theta(x) &= 2c_i \sin(\chi(x) + \omega_i).\end{aligned}\tag{A.4}$$

Demanding $\partial_1 \partial_2 \theta(x) = \partial_2 \partial_1 \theta(x)$ leads to the constraints

$$\frac{c_i}{c_i^3} = a, \quad \omega_1 = \omega_2 = 0,\tag{A.5}$$

which imply

$$\begin{aligned}\partial_i \chi(x) &= 2c_i^3 [1 + a \cot \theta(x) \cos \chi(x)], \\ \partial_i \theta(x) &= 2c_i^3 a \sin \chi(x).\end{aligned}\tag{A.6}$$

These equations can be satisfied only if χ and θ are functions of $z = c_i^3 x_i$, i.e. if they are plane waves with

$$\begin{aligned}\partial_z \chi(z) &= 2[1 + a \cot \theta(z) \cos \chi(z)], \\ \partial_z \theta(z) &= 2a \sin \chi(z).\end{aligned}\tag{A.7}$$

Since both χ and θ depend on z only, we may also consider χ as a function of θ which then leads to

$$\partial_\theta \chi(\theta) = \frac{1}{a \sin \chi(\theta)} + \cot \theta \cot \chi(\theta).\tag{A.8}$$

This can be cast into the form

$$-\partial_\theta \cos \chi(\theta) = \frac{1}{a} + \cot \theta \cos \chi(\theta),\tag{A.9}$$

and is solved by

$$\cos \chi(\theta) = \frac{\cos \theta - \lambda}{a \sin \theta},\tag{A.10}$$

where λ is an integration constant. Inserting this result in eq.(A.7) one obtains

$$\begin{aligned}-\partial_z \cos \theta(z) &= \pm 2 \sqrt{a^2(1 - \cos^2 \theta(z)) - (\cos \theta(z) - \lambda)^2}, \\ \partial_z \varphi(z) &= \frac{2(\cos \theta(z) - \lambda)}{\sin^2 \theta(z)}.\end{aligned}\tag{A.11}$$

The equation for $\partial_z \varphi(z)$ results by combining eq.(A.2) with eq.(A.7) and eq.(A.10). The above equation for $\cos \theta(z)$ can be integrated in a straightforward manner and one obtains

$$\begin{aligned}\cos \theta(z) &= \frac{1}{1 + a^2} \left[\lambda + a \sqrt{1 + a^2 - \lambda^2} \cos \left(2\sqrt{1 + a^2}(z - z_0) \right) \right] \\ &= \frac{1}{\sqrt{1 + a^2}} \left[\cos \eta + a \sin \eta \cos \left(2\sqrt{1 + a^2}(z - z_0) \right) \right].\end{aligned}\tag{A.12}$$

Here we have expressed the integration constant as

$$\lambda = \sqrt{1+a^2} \cos \eta. \quad (\text{A.13})$$

It will turn out that η is the angle between the direction \vec{j} perpendicular to the spiral plane and the 3-axis. Furthermore, one obtains

$$\begin{aligned} \sin \theta(z) \cos(\varphi(z) - \varphi(z_0)) &= \frac{1}{\sqrt{1+a^2}} \left[\sin \eta - a \cos \eta \cos \left(2\sqrt{1+a^2}(z - z_0) \right) \right], \\ \sin \theta(z) \sin(\varphi(z) - \varphi(z_0)) &= \frac{a}{\sqrt{1+a^2}} \sin \left(2\sqrt{1+a^2}(z - z_0) \right), \end{aligned} \quad (\text{A.14})$$

and thus

$$\varphi(z) - \varphi(z_0) = \text{atan} \left(\frac{a \sin \left(2\sqrt{1+a^2}(z - z_0) \right)}{\sin \eta - a \cos \eta \cos \left(2\sqrt{1+a^2}(z - z_0) \right)} \right). \quad (\text{A.15})$$

Differentiating this equation with respect to z , it is straightforward to show that eq.(A.11) is indeed satisfied.

We now form the scalar product of the unit-vector

$$\vec{e}(z) = (\sin \theta(z) \cos \varphi(z), \sin \theta(z) \sin \varphi(z), \cos \theta(z)), \quad (\text{A.16})$$

describing the staggered magnetization, with the unit-vector

$$\vec{j} = (\sin \eta \cos \varphi(z_0), \sin \eta \sin \varphi(z_0), \cos \eta), \quad (\text{A.17})$$

which yields

$$\begin{aligned} \vec{e}(z) \cdot \vec{j} &= \sin \theta(z) \sin \eta (\cos \varphi(z) \cos \varphi(z_0) + \sin \varphi(z) \sin \varphi(z_0)) + \cos \theta(z) \cos \eta \\ &= \sin \theta(z) \sin \eta \cos(\varphi(z) - \varphi(z_0)) + \cos \theta(z) \cos \eta = \frac{1}{\sqrt{1+a^2}}, \end{aligned} \quad (\text{A.18})$$

i.e. a constant (z -independent) scalar product. This finally proves that $\vec{e}(z)$ indeed describes a spiral in a plane perpendicular to \vec{j} . Replacing $z = c_i^3 x_i$ and using eq.(A.5), the wave number of the spiral (i.e. the spiral pitch) can be identified as

$$k = 2\sqrt{1+a^2} \sqrt{c_i^3 c_i^3} = 2\sqrt{c_i^3 c_i^3 + c_i c_i}. \quad (\text{A.19})$$

The particular spiral configuration considered in eq.(3.4) has $\eta = 0$ such that

$$\begin{aligned} \cos \theta(z) &= \frac{1}{\sqrt{1+a^2}} = \cos \theta_0, \\ \sin \theta(z) \sin(\varphi(z) - \varphi(z_0)) &= \frac{a}{\sqrt{1+a^2}} \sin \left(2\sqrt{1+a^2}(z - z_0) \right) \Rightarrow \\ \varphi(z) - \varphi(z_0) &= -2\sqrt{1+a^2} c_i^3 x_i = k_i x_i. \end{aligned} \quad (\text{A.20})$$

This is indeed consistent with eq.(3.8) which implies

$$a = -\tan \theta_0, \quad k_i = -\frac{2c_i^3}{\cos \theta_0}. \quad (\text{A.21})$$

References

- [1] J. C. Bednorz and K. A. Müller, *Z. Phys.* B64 (1986) 189.
- [2] W. F. Brinkman and T. M. Rice, *Phys. Rev.* B2 (1970) 1324.
- [3] J. E. Hirsch, *Phys. Rev. Lett.* 54 (1985) 1317.
- [4] P. W. Anderson, *Science* 235 (1987) 1196.
- [5] C. Gros, R. Joynt, and T. M. Rice, *Phys. Rev.* B36 (1987) 381.
- [6] S. A. Trugman, *Phys. Rev.* B37 (1988) 1597.
- [7] B. I. Shraiman and E. D. Siggia, *Phys. Rev. Lett.* 60 (1988) 740; *Phys. Rev. Lett.* 61 (1988) 467; *Phys. Rev. Lett.* 62 (1989) 1564; *Phys. Rev.* B46 (1992) 8305.
- [8] J. R. Schrieffer, X. G. Wen, and S. C. Zhang, *Phys. Rev. Lett.* 60 (1988) 944; *Phys. Rev.* B39 (1989) 11663.
- [9] S. Chakravarty, B. I. Halperin, and D. R. Nelson, *Phys. Rev.* B39 (1989) 2344.
- [10] H. Neuberger and T. Ziman, *Phys. Rev.* B39 (1989) 2608.
- [11] C. L. Kane, P. A. Lee, and N. Read, *Phys. Rev.* B39 (1989) 6880.
- [12] X. G. Wen, *Phys. Rev.* B39 (1989) 7223.
- [13] D. S. Fisher, *Phys. Rev.* B39 (1989) 11783.
- [14] S. Sachdev, *Phys. Rev.* B39 (1989) 12232.
- [15] R. Shankar, *Phys. Rev. Lett.* 63 (1989) 203; *Nucl. Phys.* B330 (1990) 433.
- [16] P. W. Anderson, *Phys. Rev. Lett.* 64 (1990) 1839.
- [17] A. Singh and Z. Tešanović, *Phys. Rev.* B41 (1990) 614.
- [18] S. A. Trugman, *Phys. Rev.* B41 (1990) 892.
- [19] C. L. Kane, P. A. Lee, T. K. Ng, B. Chakraborty, and N. Read, *Phys. Rev.* B41 (1990) 2653.
- [20] V. Elser, D. A. Huse, B. I. Shraiman, and E. D. Siggia, *Phys. Rev.* B41 (1990) 6715.
- [21] E. Dagotto, R. Joynt, A. Moreo, S. Bacci, and E. Gagliano, *Phys. Rev.* B41 (1990) 9049.
- [22] B. Chakraborty, N. Read, C. Kane, and P. A. Lee, *Phys. Rev.* B42 (1990) 4819.

- [23] P. Hasenfratz and F. Niedermayer, Phys. Lett. B268 (1991) 231.
- [24] A. Auerbach and B. E. Larson, Phys. Rev. B43 (1991) 7800.
- [25] S. Sarker, C. Jayaprakash, H. R. Krishnamurthy, and W. Wenzel, Phys. Rev. B43 (1991) 8775.
- [26] R. Eder, Phys. Rev. B43 (1991) 10706.
- [27] E. Arrigoni and G. C. Strinati, Phys. Rev. B44 (1991) 7455.
- [28] J. Igarashi and P. Fulde, Phys. Rev. B45 (1992) 10419.
- [29] R. Frésard and P. Wölfle, J. Phys.: Condens. Matter 4 (1992) 3625.
- [30] P. Hasenfratz and F. Niedermayer, Z. Phys. B92 (1993) 91.
- [31] C. Kübert and A. Muramatsu, Phys. Rev. B47 (1993) 787; cond-mat/9505105.
- [32] G. C. Psaltakis and N. Papanicolaou, Phys. Rev. B48 (1993) 456.
- [33] H. Mori and M. Hamada, Phys. Rev. B48 (1993) 6242.
- [34] O. P. Sushkov, Phys. Rev. B49 (1994) 1250.
- [35] A. V. Chubukov, T. Senthil, and S. Sachdev, Phys. Rev. Lett. 72 (1994) 2089; Nucl. Phys. B426 (1994) 601.
- [36] A. V. Chubukov and K. A. Musaelian, Phys. Rev. B51 (1995) 12605.
- [37] C. Zhou and H. J. Schulz, Phys. Rev. B52 (1995) R11557.
- [38] A. V. Chubukov and D. K. Morr, Phys. Rev. B57 (1998) 5298.
- [39] N. Karchev, Phys. Rev. B57 (1998) 10913.
- [40] L. O. Manuel and H. A. Ceccatto, Phys. Rev. B61 (2000) 3470.
- [41] M. Brunner, F. F. Assaad, and A. Muramatsu, Phys. Rev. B62 (2000) 15480.
- [42] O. P. Sushkov and V. N. Kotov, Phys. Rev. B70 (2004) 024503.
- [43] V. N. Kotov and O. P. Sushkov, Phys. Rev. B70 (2004) 195105.
- [44] J. M. Tranquada, B. J. Sternlieb, J. D. Axe, Y. Nakamura, and S. Uchida, Nature 375 (1995) 561.
- [45] S. Coleman, J. Wess, and B. Zumino, Phys. Rev. 177 (1969) 2239.
- [46] C. G. Callan, S. Coleman, J. Wess, and B. Zumino, Phys. Rev. 177 (1969) 2247.
- [47] S. Weinberg, Physica 96 A (1979) 327.

- [48] J. Gasser and H. Leutwyler, Nucl. Phys. B250 (1985) 465.
- [49] H. Georgi, Weak Interactions and Modern Particle Theory, Benjamin-Cummings Publishing Company, 1984.
- [50] J. Gasser, M. E. Sainio, and A. Švarc, Nucl. Phys. B307 (1988) 779.
- [51] E. Jenkins and A. Manohar, Phys. Lett. B255 (1991) 558.
- [52] V. Bernard, N. Kaiser, J. Kambor, and U.-G. Meissner, Nucl. Phys. B388 (1992) 315.
- [53] T. Becher and H. Leutwyler, Eur. Phys. J. C9 (1999) 643.
- [54] S. Weinberg, Phys. Lett. B251 (1990) 288; Nucl. Phys. B363 (1991) 3; Phys. Lett. B295 (1992) 114.
- [55] D. B. Kaplan, M. J. Savage, and M. B. Wise, Phys. Lett. B424 (1998) 390; Nucl. Phys. B534 (1998) 329.
- [56] E. Epelbaum, W. Glöckle, and U.-G. Meissner, Nucl. Phys. A637 (1998) 107; Nucl. Phys. A684 (2001) 371; Nucl. Phys. A714 (2003) 535.
- [57] P. F. Bedaque, H.-W. Hammer, and U. van Kolck, Phys. Rev. C58 (1998) 641; Phys. Rev. Lett. 82 (1999) 463; Nucl. Phys. A676 (2000) 357.
- [58] U. van Kolck, Prog. Part. Nucl. Phys. 43 (1999) 337.
- [59] J. N. Bahcall and R. A. Wolf, Phys. Rev. 140 (1965) B1445.
- [60] A. B. Migdal, Zh. Eksp. Teor. Fiz. 61 (1971) 2210; [Sov. Phys. JETP 34 (1972) 1184].
- [61] R. F. Sawyer, Phys. Rev. Lett. 29 (1972) 382.
- [62] D. J. Scalapino, Phys. Rev. Lett. 29 (1972) 386.
- [63] G. Baym, Phys. Rev. Lett. 30 (1973) 1340.
- [64] D. K. Campbell, R. F. Dashen, and J. T. Manassah, Phys. Rev. D12 (1975) 979.
- [65] P. Hasenfratz and H. Leutwyler, Nucl. Phys. B343 (1990) 241.
- [66] H. Leutwyler, Phys. Rev. D49 (1994) 3033.
- [67] C. P. Hofmann, Phys. Rev. B60 (1999) 388; Phys. Rev. B60 (1999) 406; Phys. Rev. B65 (2002) 094430; AIP Conference Proceedings vol.623 (2002) 305.
- [68] J. M. Román and J. Soto, Int. J. Mod. Phys. B13 (1999) 755; Ann. Phys. 273 (1999) 37; Phys. Rev. B59 (1999) 11418; Phys. Rev. B62 (2000) 3300.

- [69] O. Bär, M. Imboden, and U.-J. Wiese, Nucl. Phys. B686 (2004) 347.
- [70] F. Kämpfer, M. Moser, and U.-J. Wiese, Nucl. Phys. B729 (2005) 317.
- [71] C. Brügger, F. Kämpfer, M. Moser, M. Pepe, and U.-J. Wiese, cond-mat/0606766.
- [72] B. O. Wells, Z.-X. Shen, D. M. King, M. A. Kastner, M. Greven, and R. J. Birgeneau, Phys. Rev. Lett. 74 (1995) 964.
- [73] S. La Rosa, I. Vobornik, F. Zwick, H. Berger, M. Grioni, G. Margaritondo, R. J. Kelley, M. Onellion, and A. V. Chubukov, Phys. Rev. B56 (1997) R525.
- [74] C. Kim, P. J. White, Z.-X. Shen, T. Tohyama, Y. Shibata, S. Maekawa, B. O. Wells, Y. J. Kim, R. J. Birgeneau, and M. A. Kastner, Phys. Rev. Lett. 80 (1998) 4245.
- [75] F. Ronning, C. Kim, D. L. Feng, D. S. Marshall, A. G. Loeser, L. L. Miller, J. N. Eckstein, I. Borovic, and Z. X. Shen, Science 282 (1998) 2067.
- [76] C. Brügger, F. Kämpfer, M. Pepe, and U.-J. Wiese, cond-mat/0511367.
- [77] U.-J. Wiese and H.-P. Ying, Z. Phys. B93 (1994) 147.
- [78] B. B. Beard and U.-J. Wiese, Phys. Rev. Lett. 77 (1996) 5130.